The three-regime-model for pseudo-boiling in supercritical pressure

Qingyang Wang [a,b], Xiaojing Ma [a,b], Jinliang Xu [a,b,*], Mingjia Li [c], Yan Wang [a]

[a] Beijing Key Laboratory of Multiphase Flow and Heat Transfer for Low Grade Energy Utilization, North China Electric Power University, Beijing 102206, China
[b] Key Laboratory of Power Station Energy Transfer Conversion and System, North China Electric Power University, Ministry of Education, Beijing 102206, China
[c] Key Laboratory of Thermo-Fluid Science and Engineering of Ministry of Education, School of Energy & Power Engineering, Xi'an Jiaotong University, Xi'an, Shanxi 710049, China

ABSTRACT

Supercritical pseudo-boiling (SPPB) refers to the phenomena that when heat is applied to supercritical fluid, bubble-like and vapor-film-like features appear and wall temperature peaks occur, similar to subcritical boiling (SBB). Even though SPPB was reported in 1960s~1970s, it has not been paid attention and supercritical heat transfer (SHT) is still treated with single-phase fluid assumption, introducing difficulties in accurately describing the flow and heat transfer characteristics. Here, by analogy between SPPB and SBB, a three-regime-model is proposed for SPPB, including liquid-like (LL), two-phase-like (TPL) and vapor-like (VL) regimes. The three regimes are interfaced at an onset of pseudo-boiling temperature T^- and a termination of pseudo-boiling temperature T^+, determined by thermodynamics. Thermophysical properties of LL and VL phases are evaluated using the two pseudo-boiling temperatures. Pseudo-boiling enthalpy is defined as the enthalpy difference across the temperature span from T^- to T^+, which is analogous to latent heat of evaporation in subcritical pressure. Pseudo-vapor mass quality x is calculated using bulk fluid enthalpy and fluid enthalpies at T^- and T^+. Non-dimensional parameters are proposed to reflect interactions of mass, momentum and energy between LL and VL phases. Based on the three-regime-model, SHT is re-analyzed in a different perspective from literature. We show that SHT deviates from that of single-phase convection significantly for $0 < x < 1$ corresponding to the TPL regime, indicating that SHT cannot be treated with single-phase fluid assumption under this condition. Reynolds number for LL phase (Re_{LL}) explains the non-monotonic variation of SHT versus heat fluxes. Froude number Fr explains the difference of SHT between top generatrix and bottom generatrix in horizontal tubes. Supercritical boiling number SBO and K number successfully correlate heat transfer and pressure drop for SHT in tubes, and the K number correlation has much smaller error than DB correlation. Our work establishes a new theoretical framework for SPPB and provides a new research direction for heat transfer of supercritical fluids.

© 2021 Elsevier Ltd. All rights reserved.

1. Introduction

Supercritical fluid (SF) has received great attention for a variety of applications, including thermal-power conversion [1,2], thermochemical conversion of biomass [3,4], wastewater treatment [5], multiphase chemical reactors [6,7] and hydrothermal synthesis of nano-materials [8]. Nowadays in power engineering, supercritical water and supercritical carbon dioxide (CO_2) are two important fluids operating in cycles to convert thermal energy into electric power [9–11]. For material synthesis, the chemical kinetics are different when reactants and solvents are in subcritical pressure and supercritical pressure [12–14], and catalysis in SFs has high activity and high selectivity along with easy purification of its products [14]. Moreover, petroleum alternatives such as liquid bio-oil is highly desired as a renewable energy, and the transfer hydrogenation of bio-oil in SFs is an important upgrading method to enhance its quality and stability by converting it into a stable and low acidic fuel with notably reduced oxygen content even without external hydrogen [15]. However, at this stage, large scale applications of supercritical technologies are still far, in part due to the challenges in understanding the fundamentals of SF structure [16,17].

For a pure fluid, there is a saturation temperature corresponding to each subcritical pressure, and phase change including boiling

---

* Corresponding author at: Beijing Key Laboratory of Multiphase Flow and Heat Transfer for Low Grade Energy Utilization, North China Electric Power University, Beijing 102206, China.
E-mail address: xjl@ncepu.edu.cn (J. Xu).

Nomenclature

Ac	acceleration parameter, -
Bd	bond number, -
Bo	boiling number, -
Bu	buoyancy parameter, -
C	constant, -
Ca	capillary number, -
c_p	specific heat capacity, J/kg·K
d	tube diameter, m
e	error, -
Fr	Froude number, -
f	friction factor, -
G	mass flux, kg/m^2s
g	gravitational acceleration, m/s^2
H	correction function
h	heat transfer coefficients, W/m^2K
i	enthalpy, J/kg
i_{LV}	latent heat, J/kg
Ja	Jacob number, -
K	non-dimensional number K, -
Nu	Nusselt number, -
P	pressure, Pa
Pr	prandtl number, -
q	heat flux, W/m^2
Re	reynolds number, -
SBO	supercritical boiling number, -
T	temperature, K
T^-	the onset of pseudo-boiling temperature, K
T^+	the termination of pseudo-boiling temperature, K
We	weber number, -
x	pseudo-vapor mass quality, -
z	axial location, m

Greek symbols

Δi_{pb}	pseudo-boiling enthalpy, J/kg
Δi_{st}	structural contribution in the pseudo-boiling enthalpy, J/kg
Δi_{th}	thermal contribution in the pseudo-boiling enthalpy, J/kg
ΔT	temperature difference, K
λ	thermal conductivity, W/m·K
μ	viscosity, Pa·s
ρ	density, kg/m^3
σ	surface tension, N/m

Subscripts

ave	average
b	bulk
c	critical point
exp	experiment
L	saturated liquid
L-limit	liquid-limit
pc	pseudo-critical point
ref,L	reference point for liquid-limit
ref,V	reference point for vapor-limit
sat	saturation
V	saturated vapor
V-limit	vapor-limit
w	inner wall

Acronyms

CFD	computational fluid dynamics
CHF	critical heat flux
DB	Dittus-Boelter correlation
HTD	heat transfer deterioration
LL	liquid-like
MD	molecular dynamics
NHT	normal heat transfer
SBB	subcritical boiling
SF	supercritical fluid
SHT	supercritical heat transfer
SPPB	supercritical pseudo-boiling
TPL	two-phase-like
VL	vapor-like
VOF	volume of fluid

and condensation takes place at this saturation temperature. Latent heat of evaporation characterizes how much energy is needed to completely convert saturated liquid into saturated vapor [18]. Based on classical thermodynamics, the phase change phenomena in subcritical pressure terminate at the critical point, and a fluid beyond its critical point is called SF, which is documented in textbooks as a homogeneous, continuous and single-phase fluid without bubble/droplet and interface [18]. However, the above recognition of SF is questioned by physicists, which are summarized as follows.

Non-uniform distribution of molecules: Various molecular dynamics (MD) simulations show that SF has a non-uniform structure regarding the distribution of molecules [19,20]. For example, Skarmoutsos et al. [21] studied supercritical water with a density range of $0.2\rho_c$ to $2.0\rho_c$ at $1.03T_c$ where ρ_c and T_c are the density and temperature at the critical point, respectively, and showed non-uniform density in the fluid for both high and low densities.

Identification of liquid-like and vapor-like regions: Gallo et al. [22] investigated the thermodynamic properties of supercritical water and found that the lines connecting the maxima of response functions converge into a single line when approaching the critical point, which is called the Widom line. They found that the Widom line coincides with the crossover from liquid-like (LL) region to vapor-like (VL) region clearly visible in transport properties. Simeoni et al. [23] demonstrated the transition between LL and VL fluid when crossing the Widom line using X-ray scattering. Maxim et al. [24,25] applied neutron imaging to monitor density fluctuations of supercritical water and visualized rapid density variation as the system evolved from LL to VL during isobaric heating. These studies show that SF can be either LL or VL, depending on its location in the *P-T* phase diagram, where *P* and *T* are pressure and temperature, respectively.

Pseudo-boiling phenomenon: When heat is added to SF, phenomena such as bubble-like and film-like patterns, wall temperature peak, and whistling noise may take place, which are similar to boiling in subcritical pressure and are thus termed as pseudo-boiling. Knapp and Sabersky [26] observed bubble-like feature when heating CO_2 using a 0.254 mm diameter wire at near critical pressure. The slope of $q \sim \Delta T$ curve increased significantly when bubble-like feature was observed, displaying boiling characteristic, where q is heat flux and ΔT is temperature difference between wire and CO_2. Tamba et al. [27] observed bubbles when heating supercritical CO_2 at 7.38 MPa even at a very small ΔT of 0.3 K, which is beyond the CO_2 critical pressure 7.377 MPa. Further increase of q yielded film-like pattern. The observed bubble-like and film-like patterns are very similar to nucleate boiling and film boiling in subcritical pressure, as shown in Fig. 1. Moreover, for convective heat transfer of SF in tubes, many authors observed wall temperature peaks before the fluid temperature reaches pseudo-critical point, called heat transfer deterioration (HTD) [28–30], which is similar to the critical heat flux (CHF) for subcritical boiling. Recently, similarities between supercritical pseudo-boiling and sub-
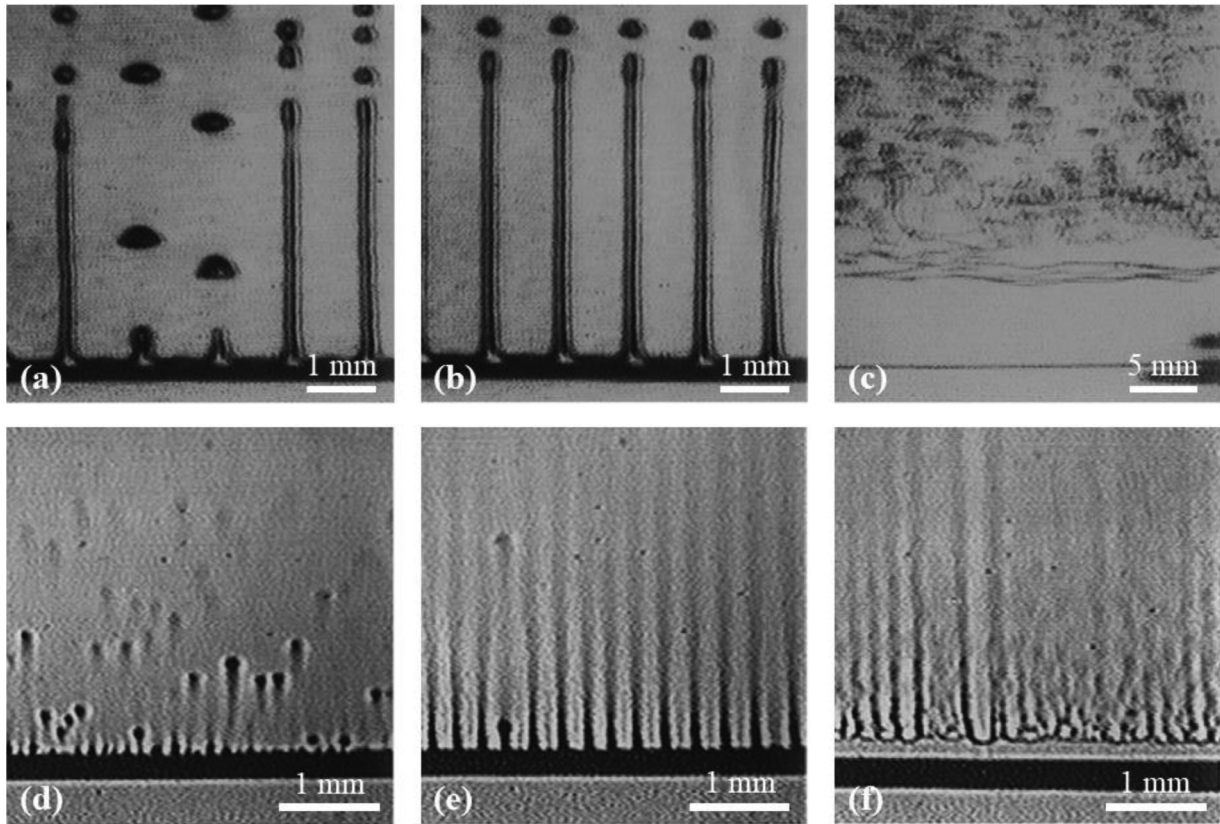
Fig. 1. Experimental images of CO_2 heated by a platinum wire at both subcritical pressure (a–c, 7.30 MPa) and supercritical pressure (d-f, 7.38 MPa), showing the similarity between subcritical boiling and supercritical heat transfer. Reproduced with permission from Ref. [27], Copyright 1998, Elsevier.
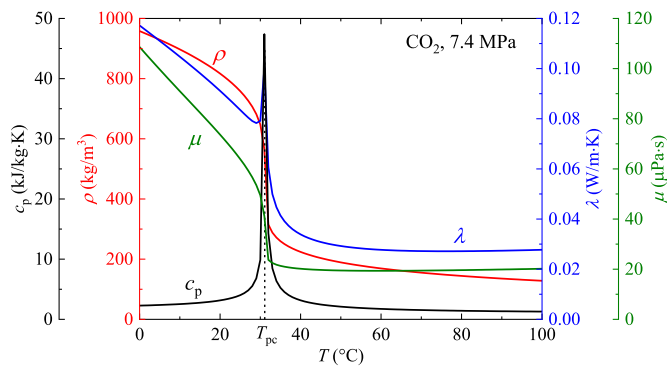

Fig. 2. Variation of thermophysical properties of CO_2 with temperatures at 7.4 MPa, showing sharp transition when crossing the pseudo-critical temperature.

critical phase change have also been acknowledged for liquid propellants used as the coolant in rocket engines, such as methane among other light hydrocarbons [31].

Even though pseudo-boiling was introduced in 1960~1970s, such concept has not received much attention. supercritical heat transfer (SHT) is still treated in a theoretical framework based on single-phase convection, and the abnormal behavior of SHT is thought to be caused by sharply varied thermophysical properties and the buoyancy/acceleration effects [28]. Fig. 2 shows CO_2 properties at a supercritical pressure of 7.4 MPa, showing the sharp variation when crossing the pseudo-critical temperature (the Widom line). Different heat transfer correlations have been proposed for SHT, which are either in the form of $Nu=CRe_{b}^{n_1}Pr_{b,ave}^{n_2}H$ [32,33], where H is a function of several correction terms of thermophysical properties characterized by inner wall tempera-

ture T_w with respect to bulk fluid temperature T_b, n_1 and n_2 are constants determined from experiments, or in the form of $Nu=CRe_{b}^{n_1}Pr_{b,ave}^{n_2}Bu^{n_3}Ac^{n_4}$ [34], where Bu and Ac are the parameters describing buoyancy effect and acceleration effect, respectively, and n_1~n_4 are constants. However, it is shown by previous investigations that: (i) Some SHT correlations are suitable in their own data range, but cannot be extended for other experimental data [34,35]. (ii) The available SHT correlations cannot adapt to different working fluids [36]. (iii) No SHT correlations exist to cover both normal heat transfer (NHT) and heat transfer deterioration (HTD) [29].

In this paper, we attempt to make an analogy between supercritical pseudo-boiling (SPPB) and subcritical boiling (SBB) and build a theoretical framework for SPPB. The paper is organized as follows: First, the theoretical framework of SBB is shortly reviewed. Then, a new theoretical framework of three-regime-model for SPPB is presented, which includes the determination of pseudo-boiling temperatures, thermophysical properties, and pseudo-boiling enthalpy. Different from SBB, SPPB has two characteristic temperatures, one for onset of pseudo-boiling (T^-), and the other for termination of pseudo-boiling (T^+). Thermophysical properties such as density, viscosity, specific heat and thermal conductivity determined at T^- and T^+ are used to characterize LL and VL phases, respectively. Pseudo-boiling enthalpy is determined as the enthalpy difference between T^+ and T^-. Based on the two sets of thermophysical properties at T^- and T^+, we introduce a new group of non-dimensional parameters for SHT. Finally, because these non-dimensional parameters characterize the mass, momentum and energy interactions between LL and VL phases, we demonstrate their successful application in characterizing SHT. Our work provides the basis for the application of SPPB concept in SHT, and can potentially benefit the industrial applications of SFs in the future.
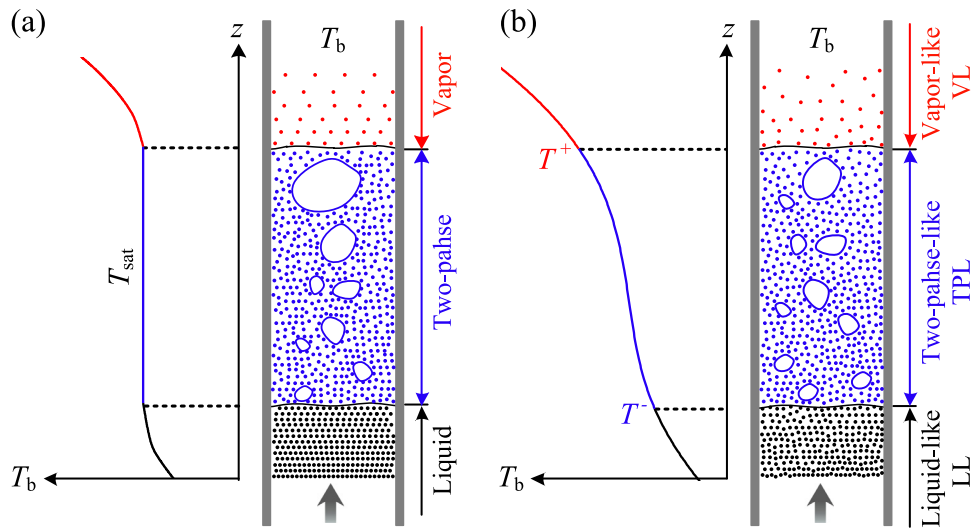
Fig. 3. The three-regime-model for (a) subcritical boiling (SBB) and (b) supercritical pseudo-boiling (SPPB). (a) SBB contains three regimes of liquid, two-phase and vapor, in which the two-phase regime occurs at a constant saturation temperature T_{sat}. (b) SPPB contains three regimes of liquid-like (LL), two-phase-like (TPL) and vapor-like (VL), which are separated by the two pseudo-boiling temperatures T^- and T^+.
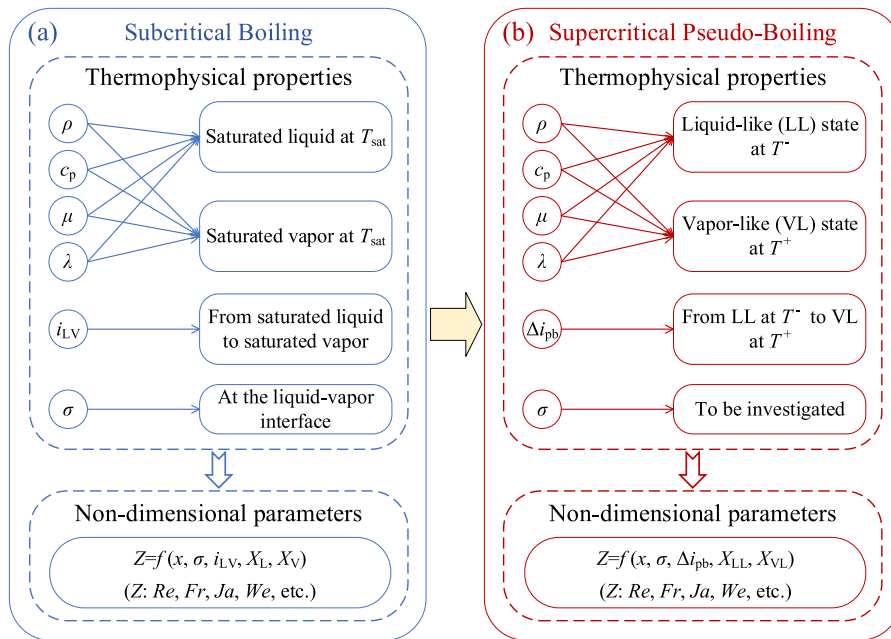

Fig. 4. The framework linking SBB and SPPB.

2. Theoretical framework for subcritical boiling (SBB)

Boiling involves phase change from liquid to vapor. Hence, boiling system belongs to a two-phase system. Figs. 3∼4 show the analogy between SBB and SPPB, with the left panels (Figs. 3a and 4a) corresponding to SBB and the right panels (Figs. 3b and 4b) corresponding to SPPB. The three-regime-model has been well established for SBB, including liquid, two-phase and vapor regimes as shown in Fig. 3a for convective boiling in tubes. Thermophysical properties, non-dimensional parameters and numerical/experimental methods are described as follows (see Fig. 4a).

Thermophysical properties: For a pure fluid, there is a saturation temperature T_{sat} corresponding to each subcritical pressure. The la-

tent heat of evaporation i_{LV} quantifies how much energy is needed to convert saturated liquid to saturated vapor. Surface tension σ characterizes the force that can stretch a curved liquid-vapor interface per unit length, which is an important property to analyze the interfacial phenomena in boiling systems.

Because boiling systems involve both saturated liquid and saturated vapor, there are two sets of thermophysical properties defined for liquid and vapor, respectively. These properties include density ρ, specific heat c_{p}, viscosity μ, thermal conductivity λ and others. Usually, the subscripts "L" and "V" represent saturated liquid and saturated vapor, respectively. Table 1 lists the relevant properties that are important for SBB.

Table 1

List of the important thermophysical properties for SBB and SPPB at a given pressure.

	Subcritical boiling (SBB)		Supercritical pseudo-boiling (SPPB)		
	Parameter	Physical meaning	Parameter	Physical meaning	How to obtain
Phase change temperature(s)	T_{sat}	SBB happens at a constant temperature	T^-, T^+	SPPB happens within a temperature range	From thermodynamic methods
Density	ρ_L, ρ_V	For each property, there are a pair of values, one for saturated liquid and one for saturated vapor	$\rho_{LL} = \rho(T^-)$ $\rho_{VL} = \rho(T^+)$	The property varies continuously with temperature, but the variation is insignificant outside of the pseudo-boiling temperature range (T^-, T^+), so a pair of values can be used to characterize LL and VL phases	Use T^- and T^+ as the reference temperatures to obtain LL and VL properties, respectively
Specific heat capacity	$c_{p,L}, c_{p,V}$		$c_{p,LL} = c_p(T^-)$ $c_{p,VL} = c_p(T^+)$		
Viscosity	μ_L, μ_V		$\mu_{LL} = \mu(T^-)$ $\mu_{VL} = \mu(T^+)$		
Thermal conductivity	λ_L, λ_V		$\lambda_{LL} = \lambda(T^-)$ $\lambda_{VL} = \lambda(T^+)$		
Phase change enthalpy	i_{LV}	Latent heat is the energy required to convert saturated liquid to saturated vapor, which contributes to expand the intermolecular distance during boiling	$\Delta i_{pb} = i(T^+) - i(T^-)$	Pseudo-boiling enthalpy is the energy required to convert LL fluid to VL fluid, which contributes both to expand the molecular structure and to heat up the fluid	Calculate the enthalpy difference between T^+ and T^-
Surface tension	σ	Surface tension represents the force per unit length at the liquid-vapor interface	$\sigma = f(\nabla T)$	Supercritical surface tension exists only when there is a temperature gradient, and its value depends on the temperature gradient	Needs further investigation

Table 2

List of non-dimensional parameters for SBB and SPPB.

Parameter	Formula in SBB	Meaning	Application	Formula in SPPB
Pseudo-vapor mass quality, x	$x = \frac{i_{ave}-i_L}{i_{LV}}$	Mass fraction of vapor phase in the two-phase mixture	Used to obtain average properties of the two-phase mixture and other non-dimensional parameters; used in correlations of two-phase flow and heat transfer	$x = \frac{i_b-i_{LL}}{\Delta i_{pb}} = \frac{i_b-i_{LL}}{i_{VL}-i_{LL}}$
Reynolds number, Re	$Re = \frac{Gd}{\mu_{ave}}$ $Re_L = \frac{G(1-x)d}{\mu_L}$ $Re_V = \frac{Gxd}{\mu_V}$	Ratio of inertia force to viscous force	Used in modeling two-phase flow and heat transfer	$Re = \frac{Gd}{\mu_b}$ $Re_{LL} = \frac{G(1-x)d}{\mu_{LL}}$ $Re_{VL} = \frac{Gxd}{\mu_{VL}}$
Froude number, Fr	$Fr = \frac{G^2}{\rho_{ave}^2 gd}$ $Fr_L = \frac{G^2(1-x)^2}{\rho_L^2 gd}$ $Fr_V = \frac{G^2 x^2}{\rho_V^2 gd}$	Ratio of inertia force to gravity force	Used in characterizing internal flow condensation or convective boiling in horizontal or inclined tubes	$Fr = \frac{G^2}{\rho_b^2 gd}$ $Fr_{LL} = \frac{G^2(1-x)^2}{\rho_{LL}^2 gd}$ $Fr_{VL} = \frac{G^2 x^2}{\rho_{VL}^2 gd}$
Jacob number, Ja	$Ja = \frac{\rho_L}{\rho_V}\frac{c_{p,L}\Delta T}{i_{LV}}$	Ratio of sensible heat to latent heat under certain superheat	Used in subcooled flow boiling to characterize the relative importance of sensible heat	$Ja = \frac{\Delta i_{rh}}{\Delta i_{st}}$
Boiling number, Bo & SBO K number, K	$Bo = \frac{q}{Gi_{LV}}$ $K = (\frac{q}{Gi_{LV}})^2 \frac{\rho_L}{\rho_V} = Bo^2 \frac{\rho_L}{\rho_V}$	Ratio of evaporation momentum force to inertia force	Used in modeling CHF of flow boiling and determining boiling regimes	$SBO = \frac{q}{Gi_{pc}}$ $K = (\frac{q}{Gi_w})^2 \frac{\rho_b}{\rho_w}$
Bond number, Bd	$Bd = \frac{g(\rho_L-\rho_V)d^2}{\sigma}$	Ratio of gravitational buoyancy force to surface tension force	Used to determine whether buoyancy force is important in microchannels	$Bd = \frac{g(\rho_{LL}-\rho_{VL})d^2}{\sigma}$
Weber number, We	$We = \frac{G^2 d}{\rho_{ave}\sigma}$	Ratio of inertia force to surface tension force	Used in correlations for two-phase flow	$We = \frac{G^2 d}{\rho_b \sigma}$
Capillary number, Ca	$Ca = \frac{\mu_L G}{\rho_L \sigma}$	Ratio of viscous force to surface tension force	Used in describing the bubble dynamics in boiling heat transfer	$Ca = \frac{\mu_{LL} G}{\rho_{LL}\sigma}$

Non-dimensional parameters: The non-dimensional parameters for SBB are listed in Table 2. At thermodynamic equilibrium state, the vapor mass quality is defined as

$$x = \frac{i_{ave} - i_L}{i_{LV}} \tag{1}$$

The x characterizes the fraction of the vapor mass relative to the total mass in a two-phase mixture. Non-dimensional parameters can be defined based on x, σ, i_{LV}, and the properties of saturated liquid and saturated vapor, characterizing important interactions of mass, momentum and energy between liquid and vapor. Some of them are described as follows.

The Reynolds number Re characterizes the importance of inertia force relative to viscous force. The bulk Re of a two-phase mixture is defined as

$$Re = \frac{Gd}{\mu_{ave}} \tag{2}$$

where G is the mass flux, d is the tube diameter, and μ_{ave} is the average viscosity defined as $\mu_{ave} = x\mu_V + (1-x)\mu_L$. The Reynolds numbers are also defined for liquid phase and vapor phase as

$$Re_L = \frac{G(1-x)d}{\mu_L}, Re_V = \frac{Gxd}{\mu_V} \tag{3}$$

The Froude number Fr characterizes the importance of inertia force relative to buoyance force. The Froude numbers for bulk, liquid phase and vapor phase are defined as

$$Fr_{ave} = \frac{G^2}{\rho_{ave}^2 gd}, Fr_L = \frac{G^2(1-x)^2}{\rho_L^2 gd}, Fr_V = \frac{G^2 x^2}{\rho_V^2 gd} \tag{4}$$

The Jacob number represents sensible heat relative to latent heat of evaporation:

$$Ja = \frac{\rho_L}{\rho_V}\frac{c_{p,L}\Delta T}{i_{LV}} \tag{5}$$

The boiling number and K number are defined as follows in Ref. [37]:

$$Bo = \frac{q}{Gi_{LV}}, K = Bo^2\frac{\rho_L}{\rho_V} = \left(\frac{q}{Gi_{LV}}\right)^2\frac{\rho_L}{\rho_V} \tag{6}$$

The Bo and K characterize evaporation momentum force relative to inertia force, but the latter further considers the density difference between the two phases. The Bo can also be regarded as a non-dimensional heat flux, linking heat flux, mass flux and working fluid together. Because Bo and K determine how easily bubbles can depart from the heated wall, they are useful for analyzing CHF of flow boiling in channels [38].

Since surface tension force is important in boiling systems, the surface tension force relative to other forces yields several non-dimensional parameters, such as

$$Bd = \frac{g(\rho_L - \rho_V)d^2}{\sigma}, Ca = \frac{\mu_L G}{\rho_L \sigma}, We = \frac{G^2 d}{\rho_L \sigma} \tag{7}$$

where the Bond number Bd represents buoyance force relative to surface tension force, the capillary number Ca represents viscous force relative to surface tension force, and the Weber number We characterizes the importance of inertia force relative to surface tension force.

Numerical simulation and experiment in boiling systems: Several numerical methods have been used to simulate boiling heat transfer. Molecular dynamics is useful to understand the basic phenomena such as bubble nucleation and growth in nanoscale [39,40]. Lattice Boltzmann method deals with boiling in mesoscale [41]. Computation fluid dynamics (CFD) is suitable to calculate boiling in macroscale [42]. Because interfacial phenomena dominate the process, the volume of fluid (VOF) method and Level-Set method are used to capture the dynamic liquid-vapor interface [42]. A large quantity of experimental database has also been accumulated for boiling heat transfer in various heater surfaces and channel geometries [43,44].

3. The three-regime-model for supercritical pseudo-boiling (SPPB)

By linking with the three-regime-model for SBB, Fig. 3b shows the newly proposed three-regime-model for SPPB, consisting of the liquid-like (LL), two-phase-like (TPL) and vapor-like (VL) regimes. The thermophysical properties and non-dimensional parameters to quantify the three-regime-model are described as follows (see Fig. 4b).

Thermophysical properties for SPPB: If one considers SHT under heating condition as a phenomenon similar to boiling in subcritical pressure, two questions may arise: (1) For SBB, a latent heat of evaporation exists. What is the pseudo-boiling enthalpy for SPPB? (2) For SBB, a saturation temperature for boiling exists. What is the pseudo-boiling temperature(s) for SPPB? These two questions are combined to be answered here.

We plot the CO_2 enthalpies versus temperature in Fig. 5, including both a subcritical curve at 6 MPa and a supercritical curve at 8 MPa. The two curves are very similar, except that boiling occurs at a constant saturation temperature T_{sat} in subcritical pressure, but pseudo-boiling occurs across a temperature span in supercritical pressure, from the onset temperature of pseudo-boiling T^- to the termination temperature of pseudo-boiling T^+.

The T^- and T^+ are determined based on thermodynamics [25,45]. The calculation method is presented in Fig. 6a for CO_2 at
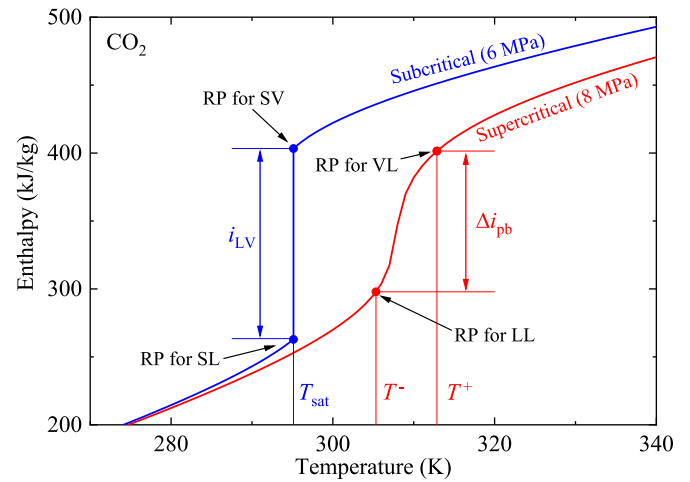

Fig. 5. Enthalpy-temperature curves for CO_2 at a subcritical pressure of 6 MPa and a supercritical pressure of 8 MPa, showing the analogy between the parameters for SBB and for SPPB. ("RP for SL" means reference point for saturated liquid, "RP for SV" means reference point for saturated vapor, "RP for LL" means reference point for liquid-like fluid, "RP for VL" means reference point for vapor-like fluid.).
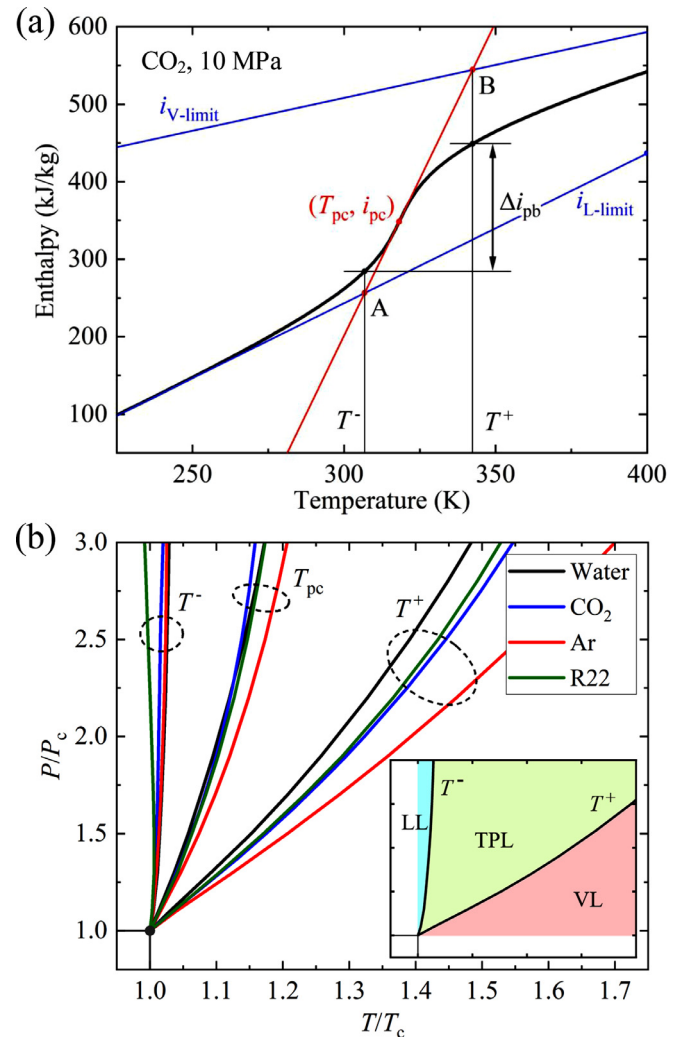

Fig. 6. (a) Calculation method for pseudo-boiling temperatures T^- and T^+ for CO_2 at 10 MPa. (b) Reduced P-T phase diagram for different supercritical fluids showing the calculated T^- and T^+ lines and the T_{pc} lines (Widom lines). Inset: the pseudo-boiling temperatures T^- and T^+ divide the supercritical region into liquid-like (LL), two-phase-like (TPL) and vapor-like (VL) regimes. (For interpretation of the references to color in this figure, the reader is referred to the web version of this article.)

10 MPa. The black curve is the enthalpy-temperature curve, with the pseudo-critical point marked by subscript "pc". The red line is the tangent line of the enthalpy curve passing through the pseudo-critical point. The two blue straight lines $i_{L\text{-limit}}$ and $i_{V\text{-limit}}$ are the liquid-limit and vapor-limit lines based on thermodynamics. The pseudo-critical tangent line can be represented by

$$i = c_{p,pc}(T - T_{pc}) + i_{pc} \tag{8}$$

where $c_{p,pc}$ and i_{pc} are specific heat and enthalpy at pseudo-critical point, respectively. The two blue lines for liquid-limit and vapor-limit are represented by

$$i_{L-limit} = c_{p,ref,L}(T - T_{ref,L}) + i_{0,L}, i_{V-\lim it} = c_{p,ref,V}(T - T_{ref,V}) + i_{0,V} \tag{9}$$

$c_{p,ref,L}$ and $i_{0,L}$ are evaluated at P_c and $T_{ref,L}{=}0.75T_c$, and $c_{p,ref,V}$ and $i_{0,V}$ are evaluated at $P{=}0$ and $T_{ref,V}{=}T_c$, where P_c and T_c are the critical pressure and temperature, respectively. The method used in this work is the same as Ref. [25], except that $T_{ref,L}{=}0.75T_c$ is used in this paper (consistent with Ref. [45], which was chosen due to practical simplicity) instead of $T_{ref,L}{=}0.5T_c$ in Ref. [25]. One practical reason is that the NIST database does not have the properties for CO_2 below certain temperature, so that calculation for CO_2 using $0.5T_c$ will fail. For water, the difference between the results obtained using these two different reference temperatures is small. For example, for water at 25 MPa, using $0.75T_c$ results in a T^- of 651.51 K while using $0.5T_c$ results in a T^- of 650.58 K, having a small difference of 0.93 K. This small temperature difference corresponds to an enthalpy difference of 16.2 kJ/kg, which accounts for only 2.35% of the pseudo-boiling enthalpy. Therefore, the choice of the reference temperature results in negligible error. The reason is because the variation of thermophysical properties is insignificant in the LL regime as long as the temperature is much smaller than T_{pc}. Thus, it is expected that the liquid-limit line is very close to the enthalpy line as shown in Fig. 6a, regardless of the reference temperature.

The three lines have two interception points A and B as shown in Fig. 6a, which determine the pseudo-boiling temperatures, with point A locating T^- and point B locating T^+. Using the method shown in Fig. 6a, we plot the supercritical phase diagram for water, CO_2, Ar (argon) and R22 (refrigerant) in Fig. 6b. At a supercritical pressure, three regimes of LL, TPL and VL are distributed in the phase diagram with $T<T^-$, $T^-<T<T^+$ and $T>T^+$, respectively, as shown in the inset of Fig. 6b, which are analogous to liquid, two-phase and vapor in subcritical pressure.

The pseudo-boiling enthalpy is the enthalpy difference within the temperature span of T^- to T^+:

$$\Delta i_{pb} = \int_{T^-}^{T^+} c_p dT = i(T^+) - i(T^-) \tag{10}$$

We present the enthalpy curve of CO_2 in Fig. 7a for both subcritical and supercritical pressure ranges. It is interesting to note the near-symmetrical distribution of i_{LV} in subcritical pressure and Δi_{pb} in supercritical pressure against the critical pressure. Different from subcritical pressure conditions, Δi_{pb} can be decoupled into a sensible heat part (Δi_{th}) and a structural transition part (Δi_{st}), as shown in Fig. 7b. The Δi_{th} serves to increase the fluid temperature, which is calculated as

$$\Delta i_{th} = c_{p,ref,L}(T^+ - T^-) \tag{11}$$

The Δi_{st} is used to expand the distance between molecules during pseudo-boiling, serving the same function as latent heat of evaporation in subcritical pressure, which can be calculated by $\Delta i_{st}{=}\Delta i_{pb}{-}\Delta i_{th}$.

Fig. 7c shows the fractions of Δi_{th} and Δi_{st} in Δi_{pb} varying with the supercritical pressure. With increasing pressure, the fraction of Δi_{th} increases and the fraction of Δi_{st} decreases. The $\Delta i_{st}/\Delta i_{pb}$ attains $\sim$0.25 at $2P_c$ and approaches zero at $\sim3P_c$. Hence, SHT at low supercritical pressure displays strong pseudo-boiling behavior which is similar to SBB, which explains why some authors observed bubble-like patterns at near critical pressure [26,27]. The pseudo-boiling effect is still significant at $\sim2P_c$, but will be weakened and become negligible at an ultra-high pressure of $3P_c$, agreeing with the conclusion drawn in Ref. [45].

Using T^- and T^+ as the reference temperatures, we further determine the thermophysical properties for LL and VL phases. Fig. 8 plots the thermophysical properties including ρ, μ, c_p and λ at both subcritical and supercritical pressures, which show near symmetrical distribution against the critical pressure. In both pressure ranges, each thermophysical property has two sets of values, one for saturated liquid and the other for saturated vapor in subcritical pressure, and one for LL phase and the other for VL phase in supercritical pressure, showing analogous behavior between subcritical and supercritical conditions. The pseudo-boiling temperatures, the pseudo-boiling enthalpy, and the thermophysical properties for LL and VL phases are listed in Table 1 in comparison with their subcritical counterparts.

Non-dimensional parameters: The non-dimensional parameters for SPPB are listed in Table 2, in analogous to those for SBB. Since some non-dimensional numbers (such as Nu and Pr) are already commonly used in SHT and do not have ambiguity in their definitions, we do not include them in Table 2.

The first non-dimensional parameter for SHT is the pseudo-vapor mass quality x, which is defined based on thermodynamics as

$$x = \frac{i_b - i_{LL}}{\Delta i_{pb}} = \frac{i_b - i_{LL}}{i_{VL} - i_{LL}} \tag{12}$$

Where i_b is the bulk fluid enthalpy. The x represents pseudo-vapor mass relative to total mass for SF.

The Jacob number is defined as the ratio of Δi_{th} to Δi_{st}, characterizing sensible heat relative to structural transition energy in the pseudo-boiling enthalpy:

$$Ja = \frac{\Delta i_{th}}{\Delta i_{st}} \tag{13}$$

The Ja can be used to characterize the importance of pseudo-boiling at different supercritical pressures: small Ja at low supercritical pressure indicates significant pseudo-boiling effect, while large Ja at high supercritical pressure represents negligible pseudo-boiling effect and near single-phase characteristics.

Because a supercritical fluid in a temperature span of T^- and T^+ is assumed to behave two-phase-like containing LL and VL phases, thermophysical properties defined at T^- and T^+ reflect mass, momentum and energy interaction between LL and VL. Hence, Reynolds numbers for bulk, LL, and VL phases are defined in the following forms

$$Re = \frac{Gd}{\mu_b}, Re_{LL} = \frac{G(1-x)d}{\mu_{LL}}, Re_{VL} = \frac{Gxd}{\mu_{VL}} \tag{14}$$

In Eq. (14), μ_b, μ_{LL}, μ_{VL} are evaluated at bulk temperature T_b, the onset of pseudo-boiling temperature T^- and the termination of pseudo-boiling temperature T^+, respectively. We note that Re is widely used to deal with SHT previously, but Re_{LL} and Re_{VL} are newly defined in this work. Similarly, the Froude numbers can be defined as

$$Fr = \frac{G^2}{\rho_b^2 gd}, Fr_{LL} = \frac{G^2(1-x)^2}{\rho_{LL}^2 gd}, Fr_{VL} = \frac{G^2 x^2}{\rho_{VL}^2 gd} \tag{15}$$

Fr, Fr_{LL} and Fr_{VL} are the bulk fluid Froude number, liquid-like Froude number and vapor-like Froude number, respectively. The
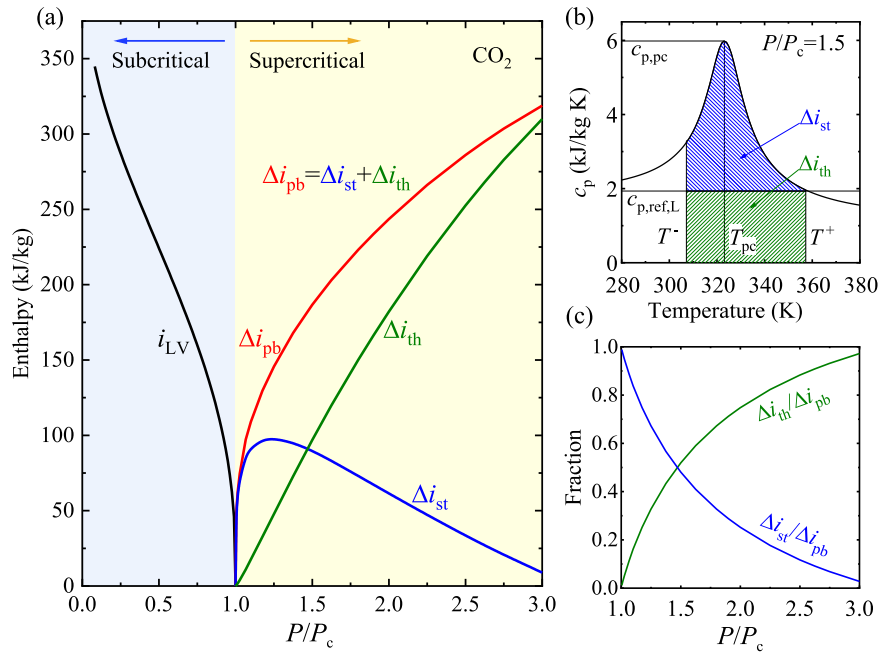
Fig. 7. (a) The analogy between latent heat of evaporation i_{LV} at subcritical pressure and pseudo-boiling enthalpy Δi_{pb} at supercritical pressure, which are nearly symmetrically distributed against the critical pressure. (b) The Δi_{pb} includes contributions from two parts: a thermal part Δi_{th} similar to sensible heat, and a structural part Δi_{st} similar to latent heat. (c) The fraction of thermal contribution Δi_{th} increases with increasing pressure, and the fraction of structural contribution Δi_{st} decreases with increasing pressure and approaches 0 at $P/P_c \sim 3$.
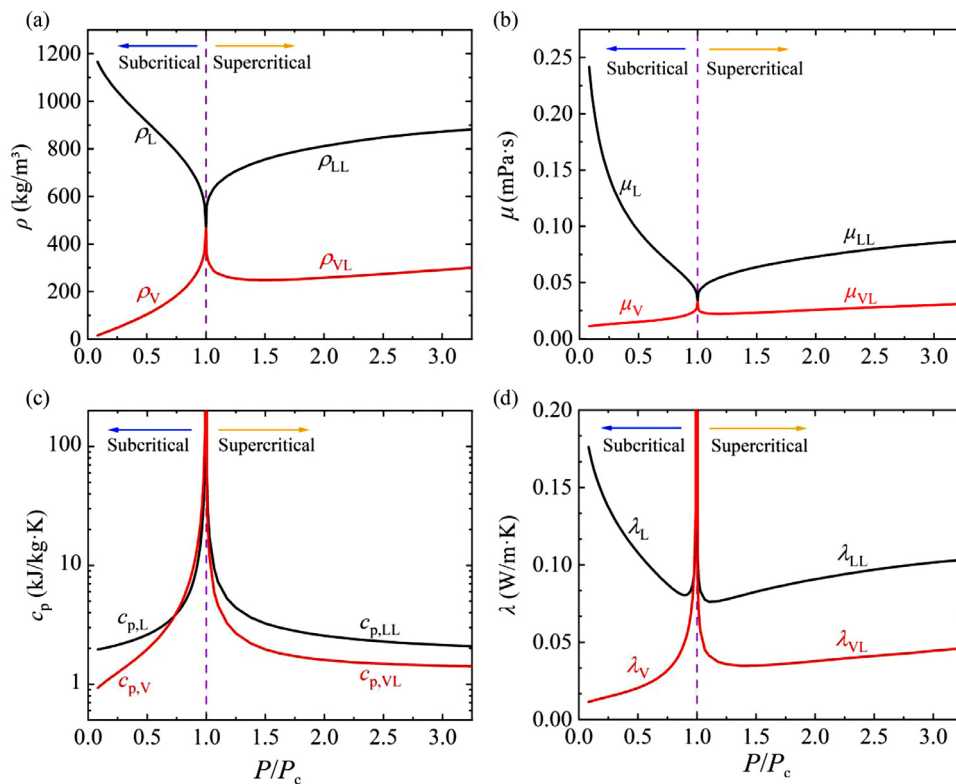
Fig. 8. The analogy of thermophysical properties at subcritical pressure and supercritical pressure. Each parameter is defined at saturated liquid state and saturated vapor state in subcritical pressure, and defined at liquid-like state and vapor-like state in supercritical pressure. The two sets of thermophysical properties are nearly symmetrically distributed against the critical pressure.

Fr characterizes the competition between inertia force and gravity force or buoyancy force. The buoyancy force exists due to the density difference between LL (heavier) fluid and VL (lighter) fluid.

Inspired by the effectiveness of boiling number and *K* number for SBB proposed by Kandlikar [37], the present authors proposed supercritical boiling number *SBO* [46] and *K* number [47] for SPPB. The motivation is to yield better understanding and prediction accuracy of CHF for SPPB. For convective heat transfer of SF in tubes under heating condition, there is a VL film attached on the wall, and LL fluid flows in the tube core. Mass transfer takes place at the interface of LL and VL phases, yielding increased VL film thickness along the flow length to deteriorate heat transfer due to low VL thermal conductivity. The mass transfer at the interface creates an evaporation momentum force to adhere VL fluid on the wall. On the other hand, inertia force due to convective flow tends to decrease the VL film thickness. The *SBO* and *K* reflect the competition between evaporation momentum force and inertia force, governing the VL film thickness to influence SHT.

$$SBO = \frac{q}{Gi_{pc}}, K = \left(\frac{q}{Gi_w}\right)^2 \frac{\rho_b}{\rho_w} \tag{16}$$

Where i_{pc} is the pseudo-critical enthalpy, and subscripts "b" and "w" represent bulk fluid condition and wall condition, respectively.

In subcritical pressure, the competition between surface tension force and other forces yields a set of non-dimensional parameters such as *Bd, Ca* and *We*. The following question arises from the analogy between SBB and SPPB: is there a surface tension force concept for SPPB? Classically, there is no surface tension in SF as it is homogeneous and has no interface. However, if one accepts the interface concept between LL and VL phases for SPPB, surface tension force does exist in supercritical pressure. Very few studies have been performed on surface tension in supercritical pressure. Using MD simulations, Tamba et al. [48] found that surface tension force is not zero under non-uniform temperature field. Hence, we accept the surface tension concept in SF. Subsequently, the following non-dimensional parameters can be defined as

$$Bd = \frac{g(\rho_{LL} - \rho_{VL})d^2}{\sigma}, Ca = \frac{\mu_{LL}G}{\rho_{LL}\sigma}, We = \frac{G^2 d}{\rho_{LL}\sigma} \tag{17}$$

Similar to subcritical conditions, the *Bd* reflects the competition between buoyancy force due to density difference between LL and VL phases and surface tension force, the *Ca* represents the competition between viscous force and surface tension force, and the *We* characterizes the competition between inertia force and surface tension force.

4. Results and discussion

Having the three-regime-model for SPPB, we then examine the usefulness of these newly defined parameters for SHT, perceiving SHT in a different angle from literature.

4.1. The pseudo-vapor mass quality x

The three-regime-model is plotted in Fig. 9 for CO_2 with reduced temperature T/T_c and reduced pressure P/P_c as two coordinates, showing the phase distribution under different supercritical pressures. The LL, TPL, and VL regimes are associated with pseudo-vapor mass quality in the ranges of $x<0$, $0<x<1$, and $x>1$, respectively. A large amount of data points have been acquired for convective heat transfer of supercritical water and CO_2 in vertical upward tubes under heating condition, including 3523 data points for supercritical water obtained from Refs. [49–58] and 3575 data points for supercritical CO_2 obtained from Refs. [59–63]. These data are re-processed and plotted as Nu/Nu_{DB} versus x in Fig. 10,
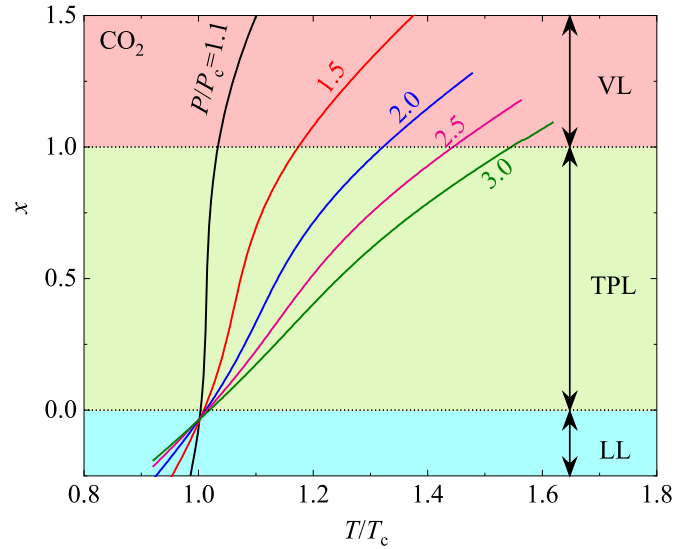

Fig. 9. The newly defined pseudo-vapor mass quality x at different pressures and temperatures for CO_2, showing that x divides the supercritical fluid into three regimes: LL ($x < 0$), TPL ($0 < x < 1$), and VL ($x > 1$).
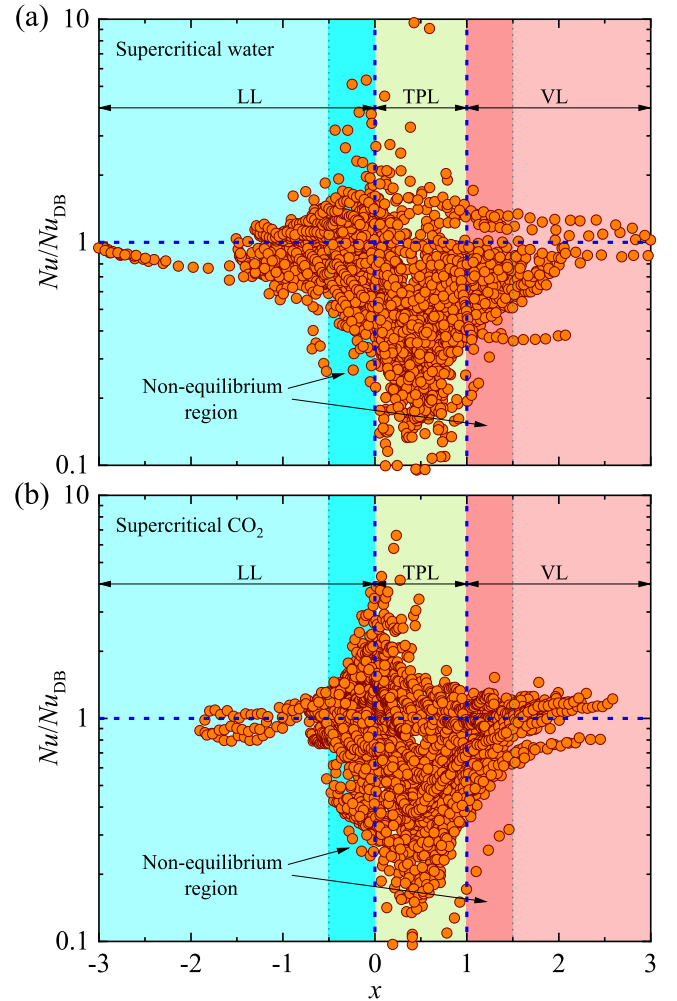

Fig. 10. Nu/Nu_{DB} versus pseudo-vapor mass quality x for (a) supercritical water and (b) supercritical CO_2, where Nu is the experimentally measured Nusselt number and Nu_{DB} is determined based on the single-phase Dittus-Boelter correlation. The Nu ratio significantly deviates from 1 in the TPL regime with $0 < x < 1$. The data points for supercritical water were obtained from Refs. [49–58] and the data points for supercritical CO_2 were obtained from Refs. [59–63].

where Nu is the experimental determined Nusselt number, and Nu_{DB} is calculated using the experimental working conditions and the Dittus-Boelter (DB) correlation:

$$Nu_{DB} = 0.023Re^{0.8}Pr^{0.4} \qquad (18)$$

where Re and Pr are determined using bulk fluid temperature. The x is determined by Eq. (12) using the bulk fluid temperature T_b and the pseudo-boiling temperatures under the corresponding experimental pressures.

$Nu/Nu_{DB}=1$ means that SHT can be exactly predicted with the single-phase DB correlation. The deviation of Nu/Nu_{DB} from 1 represents the level of deviation of SHT from single-phase fluid assumption. Nu/Nu_{DB} can be either larger than 1 corresponding to enhanced heat transfer, or smaller than 1 corresponding to deteriorated heat transfer. Fig. 10 shows that for both supercritical water (Fig. 10a) and CO_2 (Fig. 10b), the most significant deviations occur in the TPL regime with $0 < x < 1$, with the deviation as large as 10 times ($0.1 \sim 10$), indicating that SHT in this regime cannot be accurately predicted with single-phase DB correlation. In the LL regime with $-3 < x < -0.5$ and the VL regime with $x > 1.5$, the Nu/Nu_{DB} approaches 1, indicating that SHT agrees well with single-phase correlation. In the two neighboring regions to TPL ($-0.5 < x < 0$ and $1 < x < 1.5$), the Nu/Nu_{DB} still deviates from 1 although with a relatively smaller magnitude than in the TPL regime. Note that the boundaries for these two regions ($x=-0.5$ and $x=1.5$) are based on the figure and are not physically meaningful. One possible reason for this deviation is the error of the determination of pseudo-boiling temperatures T^- and T^+, which does not have unified equations among literatures as discussed before, but will definitely influence the transition boundaries of the three regimes. Another possible reason is the thermal non-equilibrium effect, while the pseudo-vapor mass quality is defined based on thermal equilibrium condition. In subcritical pressure, when heating is sufficiently strong, boiling can occur even when the bulk fluid temperature is below the saturation temperature, which is called subcooled boiling [64]. Regarding pseudo-boiling, since LL and TPL regimes are interfaced at T^-, the deviation of Nu from single-phase fluid assumption in negative x region is perhaps resulted from subcooled pseudo-boiling. That is to say, pseudo-boiling might occur with bulk fluid temperature below T^-, which requires further study. Similar reasoning can also be applied to the neighboring region with $x > 1$, where the deviation of Nu from single-phase fluid assumption may also be attributed to the local thermal non-equilibrium effect.

We further quantify the observation by calculating the relative errors of the Nu in each of the three regimes, including the mean relative error e_A, the mean absolute relative error e_R, and the root-mean-square relative error e_S. They are defined as

$$e_A = \frac{1}{n}\sum_{i=1}^{n} e_i, \quad e_R = \frac{1}{n}\sum_{i=1}^{n}|e_i|, \quad e_S = \sqrt{\frac{1}{n}\sum_{i=1}^{n} e_i^2} \qquad (19)$$

where e_i is the error for a single data point defined by

$$e_i = \frac{Nu_{DB} - Nu_{exp}}{Nu_{exp}} \qquad (20)$$

For supercritical water shown in Fig. 10a, the calculated errors for the three regimes are: in the LL regime, $e_A=15.7\%$, $e_R=24.6\%$, $e_S=41.9\%$; in the TPL regime, $e_A=152.8\%$, $e_R=157.1\%$, $e_S=230.8\%$; in the GL regime, $e_A=59.9\%$, $e_R=63.9\%$, $e_S=85.9\%$. For supercritical CO_2 shown in Fig. 10b, the calculated errors for the three regimes are: in the LL regime, $e_A=9.0\%$, $e_R=35.3\%$, $e_S=56.2\%$; in the TPL regime, $e_A=88.3\%$, $e_R=99.9\%$, $e_S=172.2\%$; in the GL regime, $e_A=20.4\%$, $e_R=28.1\%$, $e_S=46.4\%$. The errors are significantly larger in the TPL regime than in the LL and GL regimes for both fluids.

In summary, the introduction of pseudo-vapor mass quality x well explains the observation that SHT deviates from convective
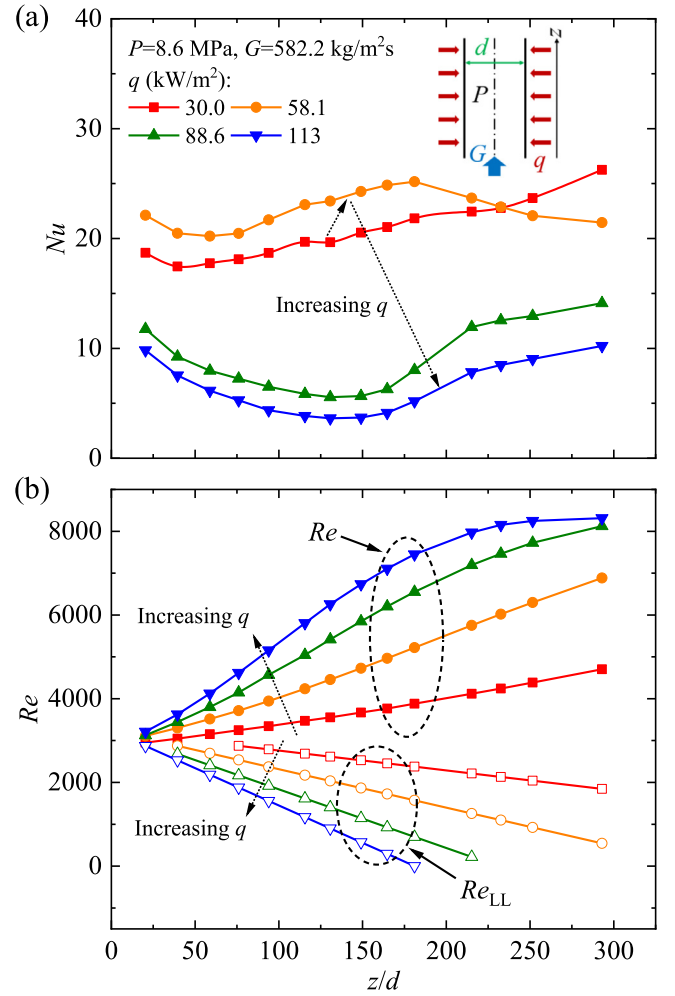

Fig. 11. (a) Variation of the Nu along the tube, showing the effect of heat flux q on Nu under vertically upward flow condition: with increase of q, Nu increases first then decreases. (b) Variation of the bulk Reynolds number Re and the liquid-like Reynolds number Re_{LL} along the tube. Although large q such as 88.6 kW/m² has large bulk Re, the corresponding Re_{LL} is small which explains the deteriorated heat transfer and laminar Nu values. The experimental data is obtained from Ref. [65].

heat transfer of single-phase fluid in the TPL regime. The deviation is caused by pseudo-boiling induced two-phase structure, which indicates that in the TPL regime, it is necessary to consider the pseudo-boiling induced two-phase effect.

4.2. The LL Reynolds number explaining laminar heat transfer characteristics

In this section, we demonstrate the effectiveness of the newly introduced Reynolds number to explain abnormal heat transfer in supercritical pressure. Fig. 11a shows the experimental results of Ref. [65] for supercritical CO_2 flowing upward in a vertical tube with an inner diameter of 0.27 mm. The Nusselt number is presented along axial flow direction z/d in Fig. 11a with $P=8.6$ MPa, $G=582.2$ kg/m²s and $q=30.0, 58.1, 88.6$ and 113.0 kW/m², which is a reprint of Fig. 4a in Ref. [65]. Non-monotonic variations of Nu are observed with respect to heat flux q: with increasing q, Nu increases first from 30.0 kW/m² to 58.1 kW/m², then decreases beyond 58.1 kW/m².

To explain the non-monotonic variation, we plot both the bulk and the LL Reynolds numbers in Fig. 11b. The bulk fluid Re is widely used to correlate SHT in the literature [32,33], but it is not sufficient to explain the non-monotonic variation with respect to

heat fluxes. Fig. 11a shows that Nu is smaller than 5 with q=88.6 kW/m^2 and 113.0 kW/m^2, indicating laminar flow characteristic, which contradicts with the bulk Re in the range of 3000~8000 corresponding to transition or turbulent flow regime.

The above contradiction can be explained by introducing the liquid-like Reynolds number Re_{LL}. Along the flow direction, the bulk fluid Re increases due to the decrease of bulk fluid viscosity with increasing temperature. However, the continuous heating yields the increase of pseudo-vapor mass quality x to decrease Re_{LL} (see Eq. (14)). The laminar heat transfer characteristics at q=88.6 kW/m^2 and 113.0 kW/m^2 is consistent with the low Re_{LL} as shown in Fig. 11b, which drops to ~0 at z/d=230 with q=88.6 kW/m^2 and z/d=180 with q=113.0 kW/m^2. On the other hand, for lower heat fluxes of q=30.0 kW/m^2 and 58.1 k/m^2, limited pseudo-vapor mass quality has been achieved, so that the laminar effect of the LL phase is not serious, and the flow characteristics are not well-captured by the Re_{LL}. Instead, the bulk Re can still be used to explain the behavior at low heat fluxes, which shows higher Nu for 58.1 kW/m^2 due to the higher bulk Re, and transition or turbulent heat transfer performance is maintained.

It is worth mentioning that the demonstration of the successful application of Re_{LL} in this section is rather qualitative instead of quantitative, and the discussion is based on a single example which might not be valid for other cases. Nevertheless, the Re_{LL} provides an alternative approach to understand the abnormal heat transfer behaviors for certain cases, and a more quantitative model needs to be developed in the future.

4.3. The Froude number explaining heat transfer in horizontal tubes

In two-phase systems at subcritical pressure, the Fr characterizes the flow and heat transfer in inclined and horizontal tubes. For examples, Xing et al. [66] correlated heat transfer coefficients of R245fa under various inclination angles using Fr, and Kandlikar [67] proposed a correlation containing Fr to predict CHF of flow boiling in horizontal tubes. For SHT, the Fr has not been mentioned previously and is defined in Eq. (15) of this paper, and its usefulness is examined below by re-analyzing an example of SHT in a horizontal tube.

Fig. 12 shows the experimental results reported in Ref. [68] for supercritical water heated in a horizontal tube with an inner diameter of 26 mm and a length of 2 m, which demonstrated non-uniform heat transfer behavior along the tube circumference. Fig. 12 shows the re-analyzed results shown in the original Fig. 5b of Ref. [68], in which the h_2/h_1 is plotted against x, where h_1 and h_2 are the heat transfer coefficient at the top generatrix and the bottom generatrix of the tube, respectively. The h_2/h_1 is larger than 1, indicating that bottom generatrix has better heat transfer than top generatrix, which is because the tube bottom is flushed by heavier fluid with lower temperature while the tube top is accumulated with lighter fluid with higher temperature. Comparing results with q=200 kW/m^2 and 300 kW/m^2, it can be seen that with increasing heat flux, the non-uniformity of heat transfer along tube circumference becomes more significant.

This non-uniform heat transfer can be explained using the three-regime-model and the Fr number. The Fr increases along the tube due to the decreasing bulk fluid density. In the LL regime with x<0, the Fr is small, indicating the importance of the buoyancy force due to the density variation, which results in stratification of the flow and consequently h_2/h_1 larger than 1. The h_2/h_1 increases with increasing x due to increasingly significant stratification, and reaches a peak value at x~0.2 in the TPL regime. Beyond x~0.2, the heat transfer difference along tube circumference represented by h_2/h_1 quickly decreases, due to the increasing Fr above 10 yielding the buoyancy force insignificant and the flow stratification weakened. In the VL regime with x>1, the h_2/h_1 approaches 1, under
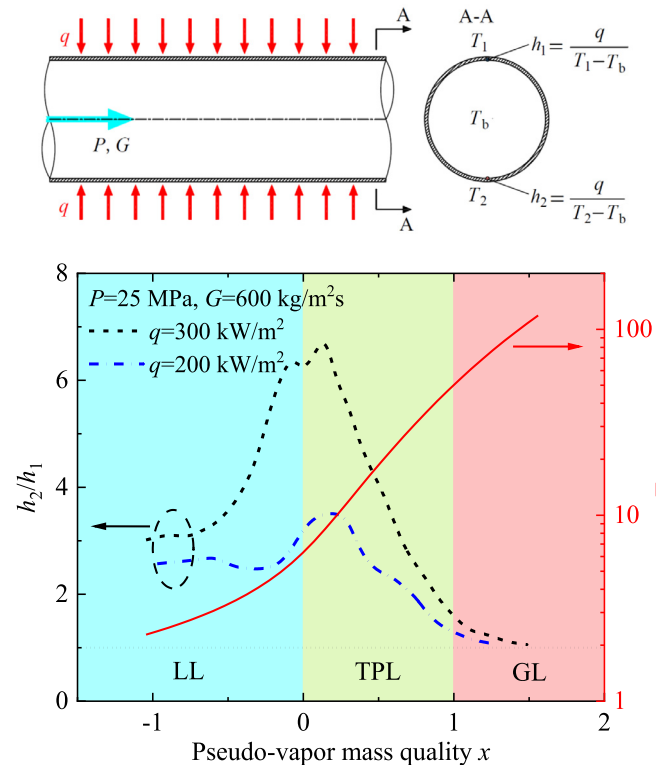

Fig. 12. Effect of Fr on the heat transfer difference between top generatrix and bottom generatrix in a horizontal tube, showing decreased difference following the beginning of TPL due to the increased Fr. The difference is weak in VL due to significantly large Fr. The experimental results were obtained from Ref. [68].

which inertia force fully suppresses buoyancy force indicated by the large Fr.

4.4. Supercritical boiling number and K number for supercritical heat transfer

According to the SPPB concept, in SHT, HTD occurs due to the thickening of the VL film near the wall similar to subcritical CHF, which is associated with wall temperature overshoot [28,29]. The growth of VL layer is governed by the competition between the evaporation momentum force and the inertia force [46], in which the former tends to adhere the VL film on the wall, while the latter tends to decrease the VL layer thickness. The SBO and K number represent the competition between these two forces.

Based on experimental results of supercritical CO_2 flowing upward inside a vertical tube with inner diameter d=10 mm, combined with the experimental results reported in the literature with d=2~10 mm, it was found that a critical SBO of 5.126×10^{-4} is the criterion for the transition between NHT mode and HTD modes [46], as shown in Fig. 13. Similar conclusion can be drawn for other fluids, except that different working fluids have different critical SBO, which are 2.018×10^{-4}, 1.653×10^{-4} and 1.358×10^{-4} for water, R134a and R22, respectively [69]. For CO_2 with non-uniform heating condition, the critical SBO equals to 8.908×10^{-4}, which is larger than that for uniform heating (5.126×10^{-4}), indicating suppressed HTD by non-uniform heating [70].

The SPPB concept indicates that the VL layer formed near the wall dominates SHT due to the low thermal conductivity of VL fluid. Defined by Eq. (16), the K number reflects the competition between evaporation momentum force and inertia force, which governs the growth of VL layer on the wall. Therefore, the effect of the VL layer thickness can be described by the K number, which indicates that it is reasonable to incorporate the K number into
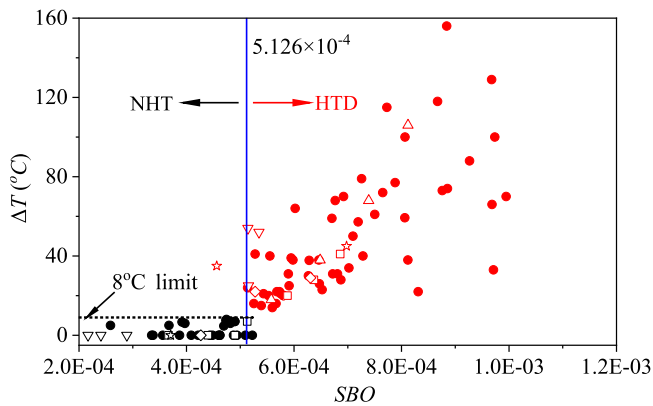
Fig. 13. For supercritical CO$_2$ heated in vertical upward tubes, a critical SBO=5.126 × 10^{-4} characterizes the transition between normal heat transfer (NHT) and heat transfer deterioration (HTD) with significant wall temperature peak. SBO represent the competition between inertia force and evaporation momentum force due to vapor-like film growth near the tube wall. Reproduced with permission from Ref. [46]. Copyright 2018, Elsevier.

the Nu correlation for SHT. Using 5560 data points of SHT in vertical tubes (including 2028 data points from the author's group and 3532 from 18 publications), a correlation was proposed to calculate Nusselt number [47]:

$$Nu = 0.0012Re_b^{0.9484}Pr_{b,ave}^{0.718}K^{-0.0313} \qquad (21)$$

Here, the average bulk Prandtl number $Pr_{b,ave}$ is defined as

$$Pr_{b,ave} = \frac{\mu_b}{\lambda_b}\frac{i_w - i_b}{T_w - T_b} \qquad (22)$$

Calculation of both K and $Pr_{b,ave}$ requires a wall temperature value T_w, as shown in Eqs. (16) and (22). Therefore, the calculation using the correlation of Eq. (21) requires iteration over the unknown wall temperature. At each given working condition including pressure P, mass flux G, wall heat flux q_w, tube diameter d, and the bulk fluid temperature T_b, an initial guess for T_w is given, which is then used to calculate the Nu using Eq. (21) and the corresponding heat transfer coefficient h. The new T_w is then obtained using T_b and h and compared with the initial T_w. The iteration continues until the T_w value converges.

The negative exponent for K in Eq. (21) means a larger K number suppresses heat transfer, which agrees with the physical meaning of K, since a larger K represents dominant evaporation momentum force and consequently VL layer pinning and thickening. Fig. 14 shows the comparison between the correlation in Eq. (21) and five other correlations proposed previously in the literature, demonstrating much improved prediction accuracy compared with other correlations in literature, which is suitable for both NHT and HTD and covers wide parameter ranges and working fluids.

To further prove the accuracy of this correlation, we calculate the Nu using the K number correlation (Eq. (21)) for the experimental data points shown in Fig. 10, and plot the calculated Nu against the experimental Nu in Fig. 15a. For comparison between the K number correlation and the DB correlation, we also plot the Nu_{DB} versus experimental Nu for the same data points in Fig. 15b. The errors are also calculated and shown in both panels of Fig. 15. Obviously, the K number correlation described by Eq. (21) demonstrates superior prediction accuracy for both CO$_2$ and water, with significantly reduced errors compared with the DB correlation.

Besides heat transfer, pressure drop is also important in SHT because it determines the required pumping power. Based on the SPPB concept, when SF is heated along the tube, the VL fluid flows near the wall and LL fluid flows in the tube core. Hence, it can be

expected that the two-phase distribution affects the pressure drop. Recently, an experimental study show that the pressure drop and heat transfer of supercritical CO$_2$ heated in vertical upward tubes can also be connected by using the K number [71]. A correlation for the friction factor f is proposed as

$$f = 2.15Re^{-0.342}K^{0.027} \qquad (23)$$

which also demonstrates smaller error than other correlations proposed in the literature over wide parameter ranges, and works for both NHT and HTD. It is also observed that the friction factors for HTD modes are significantly larger than for NHT modes as shown in Fig. 16a, which is attributed to the orifice contraction effect [71]: when a serious wall temperature overshoot takes place at a specific cross section of the tube, the over expansion of VL fluid creates an orifice to restrict the fluid flow, causing the rise of pressure drop. Furthermore, it is also found that for HTD conditions with multiple wall temperature peaks along the tube, the friction factors are larger compared with HTD cases with a single temperature peak, which is also due to the orifice contraction effect since the formation of multiple VL orifices induces multiple contractions on the flow [72], as shown in Fig. 16b.

5. Perspective of future studies

In classical theory, surface tension does not exist in supercritical fluids. However, pseudo-boiling is associated with various phenomena including bubble-like and vapor-film-like patterns, noise and wall temperature overshoot [26,27,46,73], which have been widely observed in SBB. These phenomena of SPPB indicate the existence of interfacial interaction between LL and VL phases. If the interfacial concept is correct, there should be surface tension force across the interface of LL and VL phases. Besides, bubbles have been observed in supercritical fluid for pressure slightly above the critical pressure (see Fig. 1) [27], which is a direct evidence for non-zero surface tension force in supercritical fluid.

Tamba et al. [48] performed MD simulation on supercritical Lennard-Jones fluid under non-uniform temperature field, and obtained non-zero surface tension for Ar at pressures above the critical pressure, as shown in Fig. 17. When temperature gradient exists, MD simulations at supercritical pressure reproduced a structure similar to subcritical liquid-vapor interface. The characteristics are compared with a subcritical liquid-vapor interface, and the supercritical interfacial tension value agrees with experimental measurement obtained using subcritical hydrodynamic instability model and assuming linear relationship between temperature gradient and surface tension. This study shows that an interface exists even in supercritical fluid and the interfacial tension has significant effect on SHT.

Surface tension is a very important concept and parameter to generalize a complete theoretical framework for SPPB, linking SPPB with SBB. Hence, future studies are strongly recommended on the surface tension effect in supercritical fluids, including both experimental measurements and numerical simulations.

For two-phase flow and heat transfer in subcritical pressures, various experimental methods have been well established to investigate flow patterns such as bubbly flow, slug flow, churn flow and annular flow and interfacial parameters [43]. These methods, such as high-speed flow visualization, conductance probe, and fiber optic method, are recommended to be introduced for measurements of pseudo-boiling at supercritical pressures. Some important parameters such as T^- and T^+ and VL film thickness are to be obtained for different working fluids and operating conditions.

Moreover, even though a large quantity of experimental data has been acquired for working fluids such as water and CO$_2$, the available experimental data cover narrow ranges of pressures and temperatures [28,29,74] and are thus not sufficient. Due to the de-
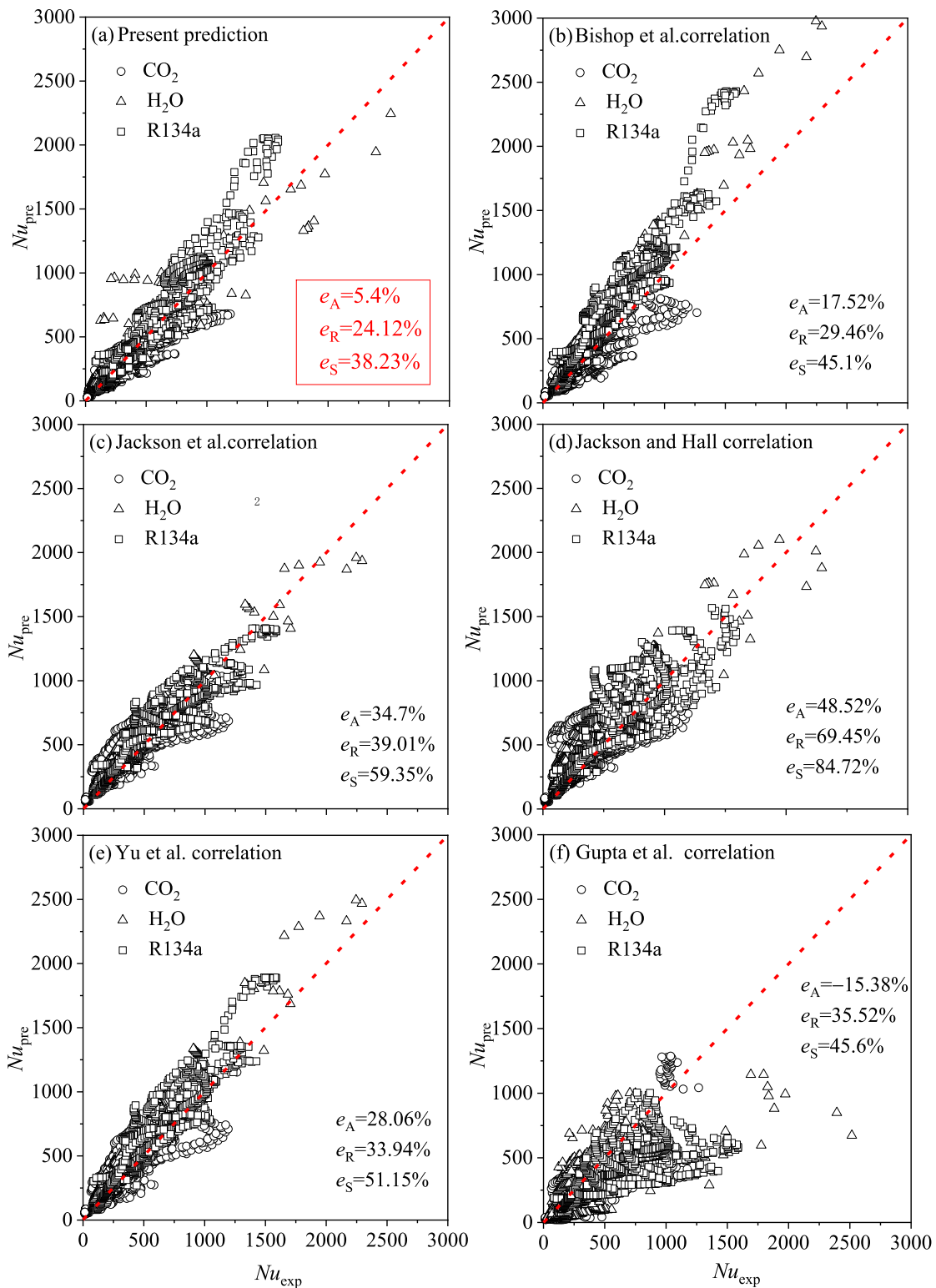
Fig. 14. Comparison of K number correlation and other correlations in the form of predicted Nu versus experimental Nu. Reproduced with permission from Ref. [47], Copyright 2019, Elsevier.

mand in the application of supercritical technologies, more SHT experiments are recommended to expand the database and provide more information on SHT characteristics. Moreover, most available literature correlated experimental data based on the single-

phase fluid assumption, and it is recommended to analyze the experimental results using the new theoretical framework of three-regime-model presented in this paper.
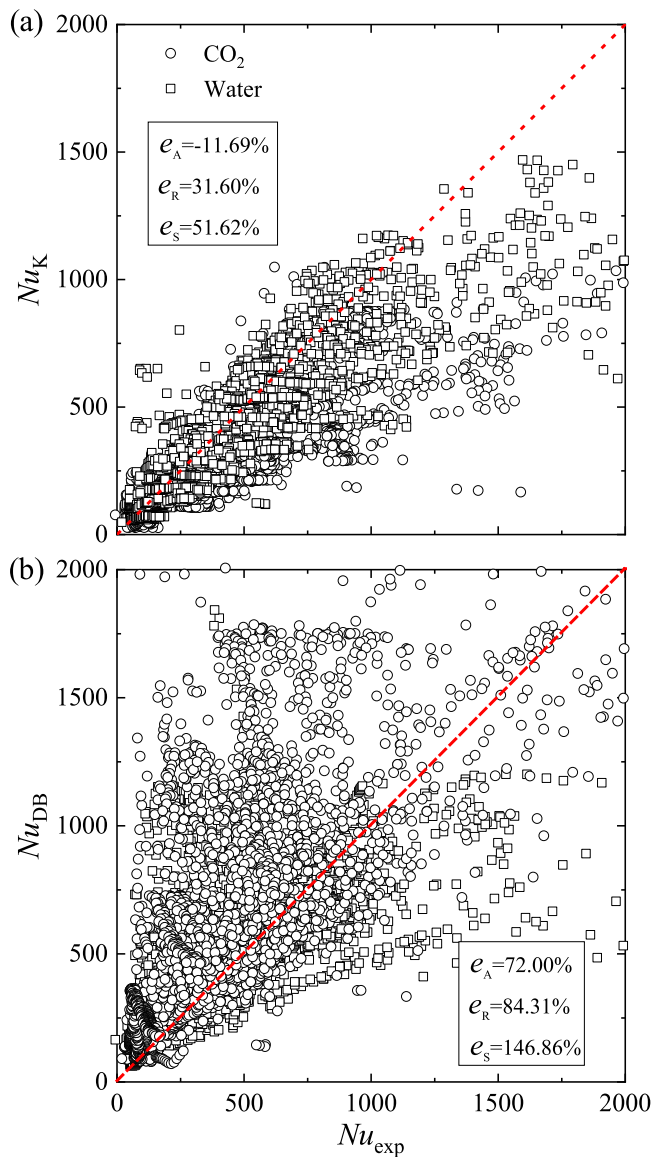
Fig. 15. (a) The Nu predicted by K number correlation (Eq. (21)) vs. experimental Nu for the data points shown in Fig. 10. (b) The Nu predicted by DB correlation (Eq. (18)) vs. experimental Nu for the data points shown in Fig. 10. The K number correlation has much smaller errors compared with the DB correlation.

6. Conclusions

SPPB has been experimentally observed decades ago, but the relevant theory is still lacking, and thorough comparison between SBB and SPPB is still missing. In this work, an analogy is performed to bridge SBB and SPPB. A three-regime-model is proposed for SPPB including LL, TPL and VL regimes, and the theoretical framework for SPPB is established. For SPPB, the onset temperature of pseudo-boiling T^- and the termination of pseudo-boiling temperature T^+ determines the boundary between the three regimes. The thermophysical properties of LL and VL phases are evaluated using these two pseudo-boiling temperatures, and the pseudo-boiling enthalpy is the difference between VL enthalpy and LL enthalpy. Based on these properties, a group of non-dimensional parameters governing the mass, momentum and energy transport are defined for SHT, and these new non-dimensional parameters such as pseudo-vapor mass quality, LL Reynolds number, Froude number, supercritical boiling number and K number are demonstrated to
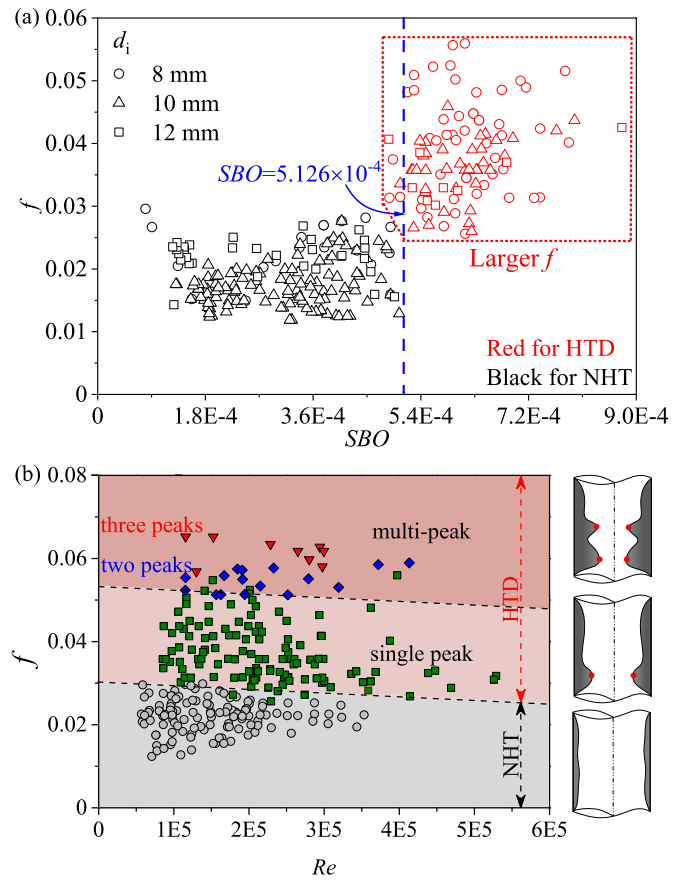

Fig. 16. (a) Friction factor f as a function of SBO, showing larger f for HTD than for NHT, due to the orifice contraction effect. Reproduced with permission from Ref. [71], Copyright 2020, Elsevier. (b) Friction factor f as a function of Re, showing large f for cases with multiple wall temperature peaks, which correspond to multiple orifice contraction effects. Reproduced with permission from Ref. [72], Copyright 2021, Elsevier.
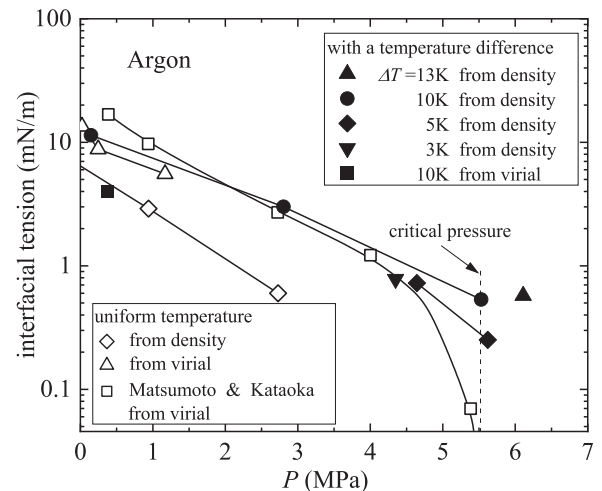

Fig. 17. Surface tension of Ar at different pressures, showing non-zero surface tension value near critical pressure and at supercritical pressure. Reproduced with permission from Ref. [48], Copyright 1997, Taylor & Francis.

successfully explain abnormal SHT characteristics. Future investigation of supercritical surface tension will fill the gap in the theoretical framework for SPPB, and enable the application of more relevant non-dimensional parameters to explain SHT. Experimental and numerical methodologies widely used in SBB are recommended to be applied for SPPB. It is also suggested that the exper-

imental database for SHT should be further expanded and the experimental results can be analyzed using the three-regime-model and the theoretical framework introduced in this work. Our work paves the way for the application of SPPB concept in SHT and will benefit the industrial applications of SFs.

Declaration of Competing Interest

None.

CRediT authorship contribution statement

Qingyang Wang: Conceptualization, Investigation, Writing – original draft. **Xiaojing Ma:** Methodology, Investigation, Writing – review & editing. **Jinliang Xu:** Conceptualization, Supervision, Funding acquisition, Writing – review & editing. **Mingjia Li:** Investigation, Validation. **Yan Wang:** Formal analysis, Investigation, Validation.

Acknowledgment

References

[1] J. Xu, E. Sun, M. Li, H. Liu, B. Zhu, Key issues and solution strategies for supercritical carbon dioxide coal fired power plant, Energy 157 (2018) 227–246.

[2] W.H. Stein, R. Buck, Advanced power cycles for concentrated solar power, Solar Energy 152 (2017) 91–105.

[3] H. Pińkowska, P. Wolak, A. Złocińska, Hydrothermal decomposition of alkali lignin in sub- and supercritical water, Chem. Eng. J. 187 (2012) 410–414.

[4] H.R. Hobbs, N.R. Thomas, Biocatalysis in supercritical fluids, in fluorous solvents, and under solvent-free conditions, Chem. Rev. 107 (6) (2007) 2786–2820.

[5] L. Qian, S. Wang, D. Xu, Y. Guo, X. Tang, L. Wang, Treatment of municipal sewage sludge in supercritical water: a review, Water Res. 89 (2016) 118–131.

[6] B. Subramaniam, R.V. Chaudhari, A.S. Chaudhari, G.R. Akien, Z. Xie, Supercritical fluids and gas-expanded liquids as tunable media for multiphase catalytic reactions, Chem. Eng. Sci. 115 (2014) 3–18.

[7] L. Guo, H. Jin, Y. Lu, Supercritical water gasification research and development in China, J. Supercrit. Fluids 96 (2015) 144–150.

[8] K.P. Johnston, P.S. Shah, Making nanoscale materials with supercritical fluids, Science 303 (5657) (2004) 482.

[9] Y. Ahn, S.J. Bae, M. Kim, S.K. Cho, S. Baik, J.I. Lee, J.E. Cha, Review of supercritical CO₂ power cycle technology and current status of research and development, Nucl. Eng. Technol. 47 (6) (2015) 647–661.

[10] F. Crespi, G. Gavagnin, D. Sánchez, G.S. Martínez, Supercritical carbon dioxide cycles for power generation: a review, Appl. Energy 195 (2017) 152–183.

[11] M.J. Li, H.H. Zhu, J.Q. Guo, K. Wang, W.Q. Tao, The development technology and applications of supercritical CO₂ power cycle in nuclear energy, solar energy and other energy industries, Appl. Therm. Eng. 126 (2017) 255–275.

[12] M. Sasaki, T. Adschiri, K. Arai, Kinetics of cellulose conversion at 25 MPa in sub- and supercritical water, AIChE J. 50 (1) (2004) 192–202.

[13] B.R. Pinkard, D.J. Gorman, E.G. Rasmussen, J.C. Kramlich, P.G. Reinhall, I.V. Novosselov, Kinetics of formic acid decomposition in subcritical and supercritical water-a Raman spectroscopic study, Int. J. Hydrog. Energy 44 (60) (2019) 31745–31756.

[14] J.M. Ha, D. Kim, J. Kim, S.K. Kim, B.S. Ahn, J.W. Kang, Supercritical-phase-assisted highly selective and active catalytic hydrodechlorination of the ozone-depleting refrigerant CHClF2, Chem. Eng. J. 213 (2012) 346–355.

[15] Y.K. Park, J.M. Ha, S. Oh, J. Lee, Bio-oil upgrading through hydrogen transfer reactions in supercritical solvents, Chem. Eng. J. 404 (2021) 126527.

[16] M.J. Cocero, Á. Cabeza, N. Abad, T. Adamovic, L. Vaquerizo, C.M. Martínez, M.V. Pazo-Cepeda, Understanding biomass fractionation in subcritical & supercritical water, J. Supercrit. Fluids 133 (2018) 550–565.

[17] A.A. Peterson, F. Vogel, R.P. Lachance, M. Fröling, J.M.J. Antal, J.W. Tester, Thermochemical biofuel production in hydrothermal media: a review of sub- and supercritical water technologies, Energy Environ. Sci. 1 (1) (2008) 32–65.

[18] Y.A. Cengel, M.A. Boles, Thermodynamics: An Engineering Approach 6th Editon (SI Units), The McGraw-Hill Companies, Inc., New York, 2007.

[19] A. Idrissi, I. Vyalov, N. Georgi, M. Kiselev, On the characterization of inhomogeneity of the density distribution in supercritical fluids via molecular dynamics simulation and data mining analysis, J. Phys. Chem. B 117 (40) (2013) 12184–12188.

[20] N. Yoshii, S. Okazaki, A large-scale and long-time molecular dynamics study of supercritical Lennard-Jones fluid. An analysis of high temperature clusters, J. Chem. Phys. 107 (6) (1997) 2020–2033.

[21] I. Skarmoutsos, J. Samios, Local density inhomogeneities and dynamics in supercritical water: a molecular dynamics simulation approach, J. Phys. Chem. B 110 (43) (2006) 21931–21937.

[22] P. Gallo, D. Corradini, M. Rovere, Widom line and dynamical crossovers as routes to understand supercritical water, Nat. Commun. 5 (1) (2014) 1–6.

[23] G. Simeoni, T. Bryk, F. Gorelli, M. Krisch, G. Ruocco, M. Santoro, T. Scopigno, The Widom line as the crossover between liquid-like and gas-like behavior in supercritical fluids, Nat. Phys. 6 (7) (2010) 503–507.

[24] F. Maxim, C. Contescu, P. Boillat, B. Niceno, K. Karalis, A. Testino, C. Ludwig, Visualization of supercritical water pseudo-boiling at Widom line crossover, Nat. Commun. 10 (1) (2019) 1–11.

[25] F. Maxim, K. Karalis, P. Boillat, D.T. Banuti, J.I. Marquez Damian, B. Niceno, C. Ludwig, Thermodynamics and dynamics of supercritical water pseudo-boiling, Adv. Sci. 8 (3) (2021) 2002312.

[26] K.K. Knapp, R.H. Sabersky, Free convection heat transfer to carbon dioxide near the critical point, Int. J. Heat Mass Transf. 9 (1) (1966) 41–51.

[27] J. Tamba, T. Takahashi, T. Ohara, T. Aihara, Transition from boiling to free convection in supercritical fluid, Exp. Therm. Fluid Sci. 17 (3) (1998) 248–255.

[28] D. Huang, Z. Wu, B. Sunden, W. Li, A brief review on convection heat transfer of fluids at supercritical pressures in tubes and the recent progress, Appl. Energy 162 (2016) 494–505.

[29] H. Wang, L.K. Leung, W. Wang, Q. Bi, A review on recent heat transfer studies to supercritical pressure water in channels, Appl. Therm. Eng. 142 (2018) 573–596.

[30] J. Xie, D. Liu, H. Yan, G. Xie, S.K. Boetcher, A review of heat transfer deterioration of supercritical carbon dioxide flowing in vertical tubes: heat transfer behaviors, identification methods, critical heat fluxes, and heat transfer correlations, Int. J. Heat Mass Transf. 149 (2020) 119233.

[31] F. Nasuti, M. Pizzarelli, Pseudo-boiling and heat transfer deterioration while heating supercritical liquid rocket engine propellants, J. Supercrit. Fluids 168 (2021) 105066.

[32] J.D. Jackson, Fluid flow and convective heat transfer to fluids at supercritical pressure, Nucl. Eng. Des. 264 (2013) 24–40.

[33] S. Gupta, E. Saltanov, S.J. Mokry, I. Pioro, L. Trevani, D. McGillivray, Developing empirical heat-transfer correlations for supercritical CO₂ flowing in vertical bare tubes, Nucl. Eng. Des. 261 (2013) 116–131.

[34] J. Yu, B. Jia, D. Wu, D. Wang, Optimization of heat transfer coefficient correlation at supercritical pressure using genetic algorithms, Heat Mass Transf. 45 (6) (2009) 757–766.

[35] M. Pizzarelli, The status of the research on the heat transfer deterioration in supercritical fluids: a review, Int. Commun. Heat Mass Transf. 95 (2018) 132–138.

[36] J. Xu, C. Liu, E. Sun, J. Xie, M. Li, Y. Yang, J. Liu, Perspective of S– CO₂ power cycles, Energy 186 (2019) 115831.

[37] S.G. Kandlikar, Heat transfer mechanisms during flow boiling in microchannels, J. Heat Transf. 126 (1) (2004) 8–16.

[38] S.G. Kandlikar, Evaporation momentum force and its relevance to boiling heat transfer, J. Heat Transf. 142 (10) (2020).

[39] W. Zhou, Y. Li, M. Li, J. Wei, W. Tao, Bubble nucleation over patterned surfaces with different wettabilities: molecular dynamics investigation, Int. J. Heat Mass Transf. 136 (2019) 1–9.

[40] L. Zhang, J. Xu, G. Liu, J. Lei, Nucleate boiling on nanostructured surfaces using molecular dynamics simulations, Int. J. Therm. Sci. 152 (2020) 106325.

[41] S. Gong, P. Cheng, Lattice Boltzmann simulations for surface wettability effects in saturated pool boiling heat transfer, Int. J. Heat Mass Transf. 85 (2015) 635–646.

[42] X. Wang, Y. Wang, H. Chen, Y. Zhu, A combined CFD/visualization investigation of heat transfer behaviors during geyser boiling in two-phase closed thermosyphon, Int. J. Heat Mass Transf. 121 (2018) 703–714.

[43] V.P. Carey, Liquid-Vapor Phase-Change Phenomena: An Introduction to the Thermophysics of Vaporization and Condensation Processes in Heat Transfer Equipment, CRC Press, 2020.

[44] S.G. Kandlikar, Handbook of phase change: boiling and condensation, Routledge (2019).

[45] D. Banuti, Crossing the Widom-line–Supercritical pseudo-boiling, J. Supercrit. Fluids 98 (2015) 12–16.

[46] B. Zhu, J. Xu, X. Wu, J. Xie, M. Li, Supercritical "boiling" number, a new parameter to distinguish two regimes of carbon dioxide heat transfer in tubes, Int. J. Therm. Sci. 136 (2019) 254–266.

[47] B. Zhu, J. Xu, C. Yan, J. Xie, The general supercritical heat transfer correlation for vertical up-flow tubes: K number correlation, Int. J. Heat Mass Transf. 148 (2020) 119080.

[48] J. Tamba, T. Ohara, T. Aihara, MD study on interfacelike phenomena in supercritical fluid, Microscale Thermophys. Eng. 1 (1997) 19–30.

[49] X. Lei, H. Li, W. Zhang, N.T. Dinh, Y. Guo, S. Yu, Experimental study on the difference of heat transfer characteristics between vertical and horizontal flows of supercritical pressure water, Appl. Therm. Eng. 113 (2017) 609–620.

[50] S. Mokry, I. Pioro, A. Farah, K. King, S. Gupta, W. Peiman, P. Kirillov, Development of supercritical water heat-transfer correlation for vertical bare tubes, Nucl. Eng. Des. 241 (4) (2011) 1126–1136.

[51] J. Pan, D. Yang, Z. Dong, T. Zhu, Q. Bi, Experimental investigation on heat transfer characteristics of water in vertical upward tube under supercritical pressure, Nucl. Power Eng. 32 (1) (2011) 75–80.

[52] K. Yamagata, K. Nishikawa, S. Hasegawa, T. Fujii, S. Yoshida, Forced convective heat transfer to supercritical water flowing in tubes, Int. J. Heat Mass Transf. 15 (12) (1972) 2575–2593.

[53] J. Ackerman, Pseudoboiling heat transfer to supercritical pressure water in smooth and ribbed tubes, J. Heat Transf. 92 (3) (1970) 490–497.

[54] J. Wang, H. Li, S. Yu, T. Chen, Investigation on the characteristics and mechanisms of unusual heat transfer of supercritical pressure water in vertically-upward tubes, Int. J. Heat Mass Transf. 54 (9) (2011) 1950–1958.

[55] S. Mokry, I. Pioro, P. Kirillov, Y. Gospodinov, Supercritical-water heat transfer in a vertical bare tube, Nucl. Eng. Des. 240 (3) (2010) 568–576.

[56] Z. Huang, Y. Li, X. Zeng, X. Yan, Z. Xiao, Experimental and numerical simulation of supercritical water heat transfer in vertical upward circular tube, At. Energy Sci. Technol. 46 (7) (2012) 799–803.

[57] Z. Shen, D. Yang, H. Xie, X. Nie, W. Liu, S. Wang, Flow and heat transfer characteristics of high-pressure water flowing in a vertical upward smooth tube at low mass flux conditions, Appl. Therm. Eng. 102 (2016) 391–401.

[58] W. Fei, Y. Jue, G. Han-yang, Z. Meng, L. Hong-bo, L. Dong-hua, Experimental research on heat transfer performance of supercritical water in vertical tube, At. Energy Sci. Technol.y 47 (6) (2013) 933.

[59] Q. Zhang, H. Li, X. Kong, J. Liu, X. Lei, Special heat transfer characteristics of supercritical CO_2 flowing in a vertically-upward tube with low mass flux, Int. J. Heat Mass Transf. 122 (2018) 469–482.

[60] N. Kline, F. Feuerstein, S. Tavoularis, Onset of heat transfer deterioration in vertical pipe flows of CO_2 at supercritical pressures, Int. J. Heat Mass Transf. 118 (2018) 1056–1068.

[61] D.E. Kim, M.-H. Kim, Experimental investigation of heat transfer in vertical upward and downward supercritical CO_2 flow in a circular tube, Int. J. Heat Fluid Flow 32 (1) (2011) 176–191.

[62] Y.Y. Bae, H.Y. Kim, D.J. Kang, Forced and mixed convection heat transfer to supercritical CO_2 vertically flowing in a uniformly-heated circular tube, Exp. Therm. Fluid Sci. 34 (8) (2010) 1295–1308.

[63] H.Y. Kim, H. Kim, J.H. Song, B.H. Cho, Y.Y. Bae, Heat transfer test in a vertical tube using CO_2 at supercritical pressures, J. Nucl. Sci. Technol. 44 (3) (2007) 285–293.

[64] G.R. Warrier, V.K. Dhir, Heat transfer and wall heat flux partitioning during subcooled flow nucleate boiling-a review, J. Heat Transf. 128 (12) (2006) 1243–1256.

[65] P.X. Jiang, Y. Zhang, C.R. Zhao, R.F. Shi, Convection heat transfer of CO_2 at supercritical pressures in a vertical mini tube at relatively low Reynolds numbers, Exp. Therm. Fluid Sci. 32 (8) (2008) 1628–1637.

[66] F. Xing, J. Xu, J. Xie, H. Liu, Z. Wang, X. Ma, Froude number dominates condensation heat transfer of R245fa in tubes: effect of inclination angles, Int. J. Multiph. Flow 71 (2015) 98–115.

[67] S.G. Kandlikar, A general correlation for saturated two-phase flow boiling heat transfer inside horizontal and vertical tubes, J. Heat Transf. 112 (1) (1990) 219–228.

[68] S. Yu, H. Li, X. Lei, Y. Feng, Y. Zhang, H. He, T. Wang, Experimental investigation on heat transfer characteristics of supercritical pressure water in a horizontal tube, Exp. Therm. Fluid Sci. 50 (2013) 213–221.

[69] J. Xu, H. Zhang, B. Zhu, J. Xie, Critical supercritical-boiling-number to determine the onset of heat transfer deterioration for supercritical fluids, Solar Energy 195 (2020) 27–36.

[70] B. Zhu, J. Xu, H. Zhang, J. Xie, M. Li, Effect of non-uniform heating on scCO₂ heat transfer deterioration, Appl. Therm. Eng. 181 (2020) 115967.

[71] H. Zhang, J. Xu, X. Zhu, J. Xie, M. Li, B. Zhu, The K number, a new analogy criterion number to connect pressure drop and heat transfer of sCO₂ in vertical tubes, Appl. Therm. Eng. 182 (2021) 116078.

[72] H. Zhang, J. Xu, Q. Wang, X. Zhu, Multiple wall temperature peaks during forced convective heat transfer of supercritical carbon dioxide in tubes, Int. J. Heat Mass Transf. 172 (2021) 121171.

[73] K. Goldmann, *Special Heat Transfer Phenomena for Supercritical Fluids*. No. NDA-2-31, Nuclear Development Corp. of America, White Plains, NY (United States), 1956.

[74] M.M. Ehsan, Z. Guan, A. Klimenko, A comprehensive review on heat transfer and pressure drop characteristics and correlations with supercritical CO_2 under heating and cooling applications, Renew. Sustain. Energy Rev. 92 (2018) 658–675.